Article

Cell Reports

The Probability of Neurotransmitter Release Governs AMPA Receptor Trafficking via Activity-Dependent Regulation of mGluR1 Surface Expression

Graphical Abstract

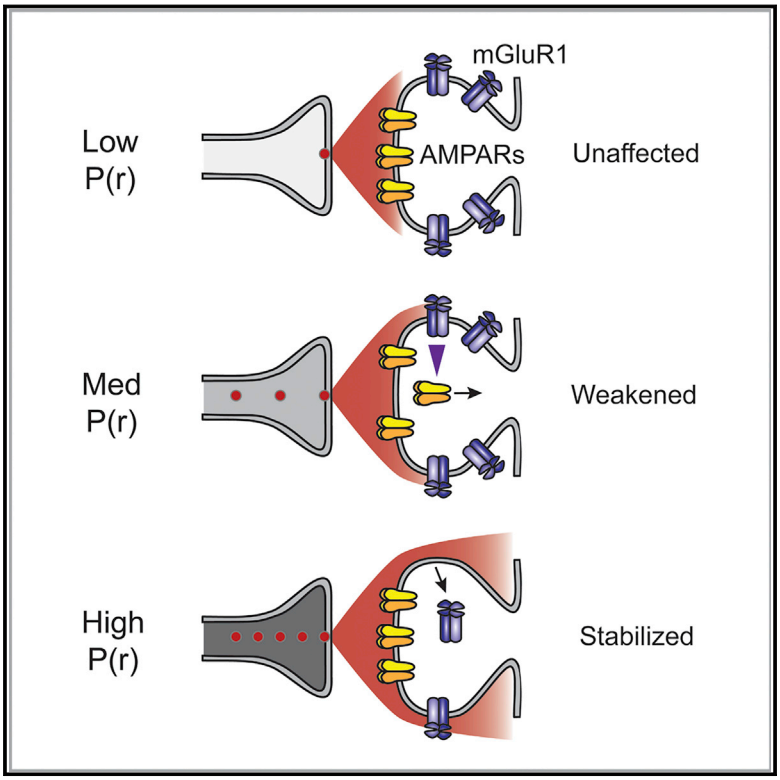

Authors

Thomas M. Sanderson, Clarrisa A. Bradley, John Georgiou, ..., Bong-Kiun Kaang, Sang Jeong Kim, Graham L. Collingridge

Correspondence

sangjkim@snu.ac.kr (S.J.K.), collingridge@lunenfeld.ca (G.L.C.)

In Brief

Synaptic strength can change in response to patterned electrical stimulation, resulting in networks that encode memories. Sanderson et al. have found that synapses don't necessarily respond the same way to identical patterns, however. The change in synaptic strength depends on the probability of neurotransmitter release, a highly variable synaptic property.

Highlights

- AMPAR trafficking can be influenced by the probability of glutamate release, P(r)
- High-P(r) synapses are protected from weakening induced by mGluR1
- Theta burst stimulation causes downregulation of mGluR1 at high-P(r) synapses
- Consequently, postsynaptic plasticity can be pre-tuned by presynaptic activity

Sanderson et al., 2018, Cell Reports *25*, 3631–3646
December 26, 2018
https://doi.org/10.1016/j.celrep.2018.12.010

CellPress

Cell Reports
Article

The Probability of Neurotransmitter Release Governs AMPA Receptor Trafficking via Activity-Dependent Regulation of mGluR1 Surface Expression

Thomas M. Sanderson,[1,2,3,5] Clarrisa A. Bradley,[1,4] John Georgiou,[5] Yun Hwa Hong,[2,6] Ai Na Ng,[3] Yeseul Lee,[1,3] Hee-Dae Kim,[7] Doyeon Kim,[7] Mascia Amici,[3] Gi Hoon Son,[8] Min Zhuo,[1,9,10,11] Kyungjin Kim,[7] Bong-Kiun Kaang,[1,10,11] Sang Jeong Kim,[1,2,6,*] and Graham L. Collingridge[1,3,5,9,12,*]

[1]Department of Brain and Cognitive Sciences, College of Natural Sciences, Seoul National University, Seoul 151-746, Korea
[2]Neuroscience Research Institute, Seoul National University College of Medicine, 28 Yeongeon-dong, Jongno-gu, Seoul 110-799, Korea
[3]School of Physiology, Pharmacology & Neuroscience, University of Bristol, Dorothy Hodgkin Building, Whitson Street, Bristol BS1 3NY, UK
[4]Neuroscience & Mental Health Program, The Hospital for Sick Children, Toronto, ON, Canada
[5]Lunenfeld-Tanenbaum Research Institute, Mount Sinai Hospital, Toronto, ON M5G 1X5, Canada
[6]Department of Physiology, Seoul National University College of Medicine, 28, Yeongeon-dong, Jongno-gu, Seoul 110-799, Korea
[7]Department of Brain and Cognitive Sciences, DGIST, and Korea Brain Institute (KBRI), Daegu, 41068, Korea
[8]Department of Biomedical Sciences, Korea University College of Medicine, Seoul 136-705, Seoul, Korea
[9]Department of Physiology, Faculty of Medicine, University of Toronto, Toronto, ON M5S 1A8, Canada
[10]Department of Biological Sciences, College of Natural Sciences, Seoul National University, Building 504, Room 202, 599 Gwanangno, Gwanak-gu 151-747, Seoul, Korea
[11]Center for Neuron and Disease, Frontier Institutes of Science and Technology, Xi'an Jiaotong University, Xi'an, 710049, China
[12]Lead Contact
*Correspondence: sangjkim@snu.ac.kr (S.J.K.), collingridge@lunenfeld.ca (G.L.C.)
https://doi.org/10.1016/j.celrep.2018.12.010

SUMMARY

A major mechanism contributing to synaptic plasticity involves alterations in the number of AMPA receptors (AMPARs) expressed at synapses. Hippocampal CA1 synapses, where this process has been most extensively studied, are highly heterogeneous with respect to their probability of neurotransmitter release, P(r). It is unknown whether there is any relationship between the extent of plasticity-related AMPAR trafficking and the initial P(r) of a synapse. To address this question, we induced metabotropic glutamate receptor (mGluR) dependent long-term depression (mGluR-LTD) and assessed AMPAR trafficking and P(r) at individual synapses, using SEP-GluA2 and FM4-64, respectively. We found that either pharmacological or synaptic activation of mGluR1 reduced synaptic SEP-GluA2 in a manner that depends upon P(r); this process involved an activity-dependent reduction in surface mGluR1 that selectively protects high-P(r) synapses from synaptic weakening. Consequently, the extent of postsynaptic plasticity can be pre-tuned by presynaptic activity.

INTRODUCTION

A primary mechanism by which information is encoded and stored in the CNS is via alterations in the number of postsynaptic AMPARs at synapses (Bredt and Nicoll, 2003; Collingridge et al., 2004; Malinow and Malenka, 2002). Neurons can receive tens of thousands of synaptic inputs that, at sites such as the Schaffer collateral-commissural inputs to CA1 pyramidal neurons, vary considerably in their release probability, P(r) (Branco and Staras, 2009; Hessler et al., 1993; Rosenmund et al., 1993). We wondered whether there is any relationship between AMPAR trafficking and P(r). We addressed this question by studying a form of long-term depression (LTD) induced by the activation of metabotropic glutamate receptors (mGluRs). This major form of synaptic plasticity is observed robustly in many areas of the brain (Collingridge et al., 2010; Lüscher and Huber, 2010), is believed to be important for learning and memory (Di Prisco et al., 2014; Eales et al., 2014; Goh and Manahan-Vaughan, 2013), and may be disrupted in a variety of disorders, including autism spectrum disorder (Auerbach et al., 2011; Bear et al., 2004; Chévere-Torres et al., 2012), Alzheimer's disease (Hsieh et al., 2006), and drug addiction (Mameli et al., 2007).

In this study, we induced mGluR-LTD by addition of the group I mGluR agonist (RS)-dihydroxyphenylglycine (DHPG) (Palmer et al., 1997), a protocol that will activate mGluRs irrespective of synapse P(r). We also activated mGluR1 synaptically by delivering theta burst stimulation (TBS) to afferent inputs. By combining, for the first time, multiphoton imaging of FM4-64 (FM) to record P(r) and SEP-GluA2 to measure AMPAR trafficking, we determined the relationship between AMPAR trafficking and P(r) at individual CA1 synapses.

DHPG application resulted in substantial LTD that was triggered by the activation of mGluR1 and was associated with a net loss of AMPARs. The extent of synaptic AMPAR loss (i.e., reductions of SEP-GluA2 puncta fluorescence adjacent to FM sites) was dependent on P(r), with the largest effect observed at low-P(r) synapses. TBS, during NMDA receptor (NMDAR) blockade, also affected AMPARs in a manner that was influenced

by P(r). Interestingly, there was no loss of SEP-GluA2 in response to either DHPG or TBS at high-P(r) synapses (>0.4). We used SEP-mGluR1 to study the basal levels and activity-dependent trafficking of this mGluR subtype. The levels of SEP-mGluR1 were reduced at high-P(r) synapses, and TBS drove its loss from the vicinity of high-P(r) synapses. Thus, we demonstrate that an activity-dependent reduction in mGluR1 provides a regulatory mechanism to protect high-P(r) synapses from mGluR1-dependent postsynaptic weakening. In this way, mGluR1 enables a rapid coordination of pre- and postsynaptic function.

RESULTS

Alterations in AMPAR Trafficking during DHPG-LTD

Since its first description (Palmer et al., 1997), DHPG has been used extensively to study LTD induced by the activation of group I mGluRs (mGluR1 and mGluR5). Multiple forms of LTD have been identified that are triggered by mGluR1 or mGluR5 and are expressed either by a decrease in P(r) or by alterations in AMPAR trafficking (reviewed in Gladding et al., 2009). It was, therefore, necessary to characterize DHPG-LTD in our preparation. In the presence of L-689,560 (10 μM), to block NMDARs, RS-DHPG (100 μM) reliably induced LTD (to 47 ± 10% of baseline, n = 6, quantified 30 min following washout of DHPG; Figures 1A and 1C), which was not associated with a change in paired-pulse facilitation (PPF; 99 ± 11% of control, n = 6; Figures 1B and 1C). In a second set of interleaved experiments, compared with control LTD (45 ± 8% of baseline, n = 8) antagonists of mGluR1, LY 367,385 (LY; 100 μM) or YM 298198 (YM; 2 μM), significantly inhibited DHPG-LTD (87 ± 9%, n = 7, $p < 0.05$, and 92 ± 12%, n = 7, $p < 0.001$, respectively; Figures 1D and S1A and S1B). However, inhibition of mGluR5, using MPEP (10 μM), had no significant effect on DHPG-LTD (55 ± 9%, n = 6, $p > 0.05$; Figures 1D and S1C). Using two-input experiments, we found that DHPG-LTD requires synaptic stimulation, although stimulation of a heterosynaptic input was sufficient (Figure S2). Similar to other studies using organotypic slices, we routinely included 10 μM 2-chloroadenosine to reduce neuronal excitability (e.g., Jo et al., 2010). However, similar observations were made in the absence of 2-chloroadenosine (i.e., mGluR5-independent, mGluR1-dependent DHPG-LTD that was not associated with changes in P(r); Figure S3). In summary, the form of DHPG-LTD investigated here is triggered by the activation of mGluR1 and expressed postsynaptically.

The vast majority of endogenous AMPARs at CA1 synapses comprise GluA2 subunits (Greger et al., 2017; Lu et al., 2009; Wenthold et al., 1996), which are essential for DHPG-LTD (Zhou et al., 2011). Here, we used super-ecliptic pHluorin-tagged GluA2 (SEP-GluA2) as a tool to image GluA2 (Figure 1E; Ashby et al., 2004, 2006). To validate its use to study LTD at CA1 synapses, we performed additional control experiments (Figures 1F–1H). Expression of SEP-GluA2 did not significantly affect synaptic strength, as assessed by comparing EPSCs in transfected and nearby non-transfected neurons, evoked by activation of the same set of afferent fibers. For SEP-GluA2 and control, respectively, the AMPAR/NMDAR ratios (1.1 ± 0.1, n = 10, and 1.2 ± 0.2, n = 8 pairs; Figure 1F) and the absolute AMPAR EPSC amplitudes (165 ± 35 and 130 ± 30 pA, n = 10 pairs, respectively; Figure 1G) were similar ($p > 0.05$). Importantly, SEP-GluA2 did not affect the ability of the synapses to express LTD, as DHPG induced similar levels of depression in SEP-GluA2-expressing neurons and non-transfected control neurons (62 ± 5%, n = 6, and 57 ± 14%, n = 5, respectively, $p > 0.05$; Figure 1H). These results show that SEP-GluA2 can accurately report AMPAR trafficking during mGluR-induced synaptic plasticity at CA1 synapses.

On imaging SEP-GluA2 at individual puncta, we found that under control conditions, SEP-GluA2 fluorescence was stable on average over the duration of the experiments, with a similar number of puncta increasing and decreasing in intensity (Figures 1I–1K, black lines). As expected, application of NMDA (50 μM, 5 min) led to a decrease in the fluorescence of most puncta, resulting in a large leftward shift in the cumulative likelihood distribution compared with the interleaved controls ($p < 0.001$, Kolmogorov-Smirnov [K-S] test; Figure 1I-J, orange line). However, application of DHPG had a smaller and bimodal effect on AMPAR trafficking; approximately 60% of spines decreased in fluorescence ($p < 0.001$, K-S test; Figures 1I and 1K), while others increased in intensity, compared with interleaved controls (Figure 1K, inset). In summary, NMDA and DHPG mediate qualitatively and quantitatively different actions on SEP-GluA2 fluorescence, suggestive of different underlying trafficking mechanisms.

AMPAR Trafficking Depends on P(r)

Given that synaptic activity can modulate DHPG-LTD expression, we next investigated whether the extent of AMPAR trafficking was related to the level of presynaptic activity at individual synapses. To address this question, we adapted methods that use FM dyes in dissociated culture (Murthy et al., 1997) and approaches to reduce background staining (Kay et al., 1999; Pyle et al., 1999) so that we could measure both FM and SEP-GluA2 at the same synapses within hippocampal slices (Figure 2A). We selected a red fluorescent dye, FM 4-64 (FM), that could be imaged simultaneously with the green emission of SEP-GluA2. This combination of two well-established techniques enabled us to address, for the first time, the relationship between AMPAR dynamics and P(r) at individual synapses. We confirmed that FM staining was activity dependent, as FM was de-stained by further synaptic stimulation (Figure 2A). The effects of DHPG on SEP-GluA2 fluorescence were similar at FM-positive and FM-negative sites (Figures 2B–2D), which is consistent with the observation that although DHPG-LTD requires synaptic stimulation, it is not input specific (Figure S2).

Because vesicles are labeled with FM only when a successful release event has occurred, FM uptake can also be used to estimate P(r) at synapses (Murthy et al., 1997; Figures 2E–2G), enabling us to determine whether there is a correlation between the magnitude of the SEP-GluA2 fluorescence change and P(r). Under control conditions, recorded over a 30 min period, the baseline SEP-GluA2 fluorescence fluctuations were entirely independent of P(r) (Spearman's $r_s = -0.06$, $p > 0.05$, n = 59 synapses from nine cells; Figure 2H). In contrast, when slices were treated with DHPG, the changes in SEP-GluA2 at individual synapses, over an equivalent time period, were correlated with their initial P(r) (Spearman's $r_s = 0.48$, $p < 0.001$, n = 56 synapses from eight cells; Figure 2I). Surprisingly, the receptor loss occurred predominantly at low-P(r) synapses.

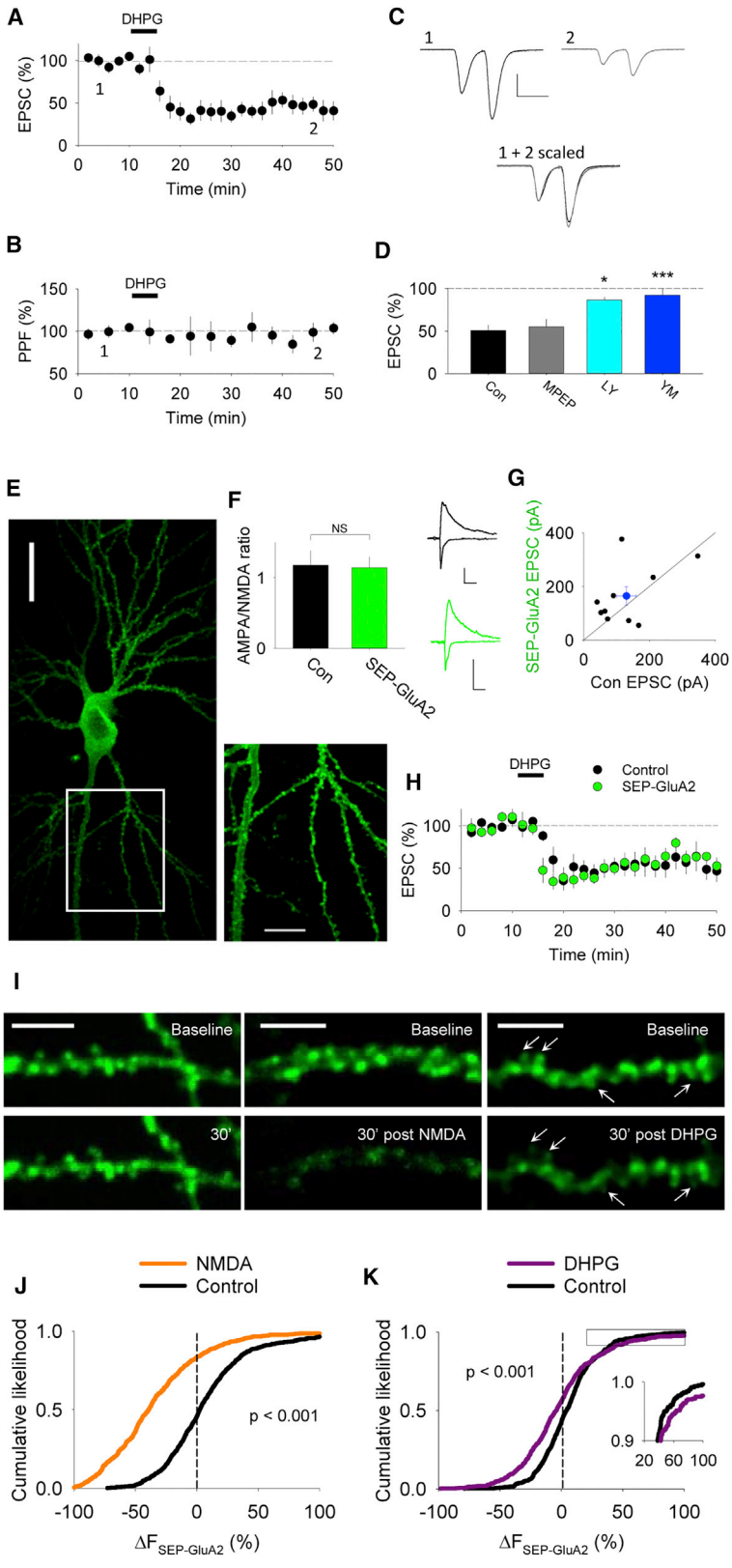

Figure 1. DHPG-LTD Involves Internalization of AMPARs

(A) DHPG (100 μM, 5 min) induced LTD with no alteration in PPF (n = 6). In this and subsequent patch-clamp experiments, each point represents the mean and the error bars the SEM of n experiments, each from a separate organotypic slice. Each measurement is the average of four successive EPSC amplitudes. DHPG was applied for the time indicated by the black bar. The NMDAR glycine-site antagonist L-689,560 (10 μM) was applied at least 20 min prior to and during DHPG application.

(B) A corresponding plot of the PPF, calculated for 4 min epochs during the DHPG experiment shown in (A).

(C) Sample traces for baseline (1) and after DHPG-LTD (2) and peaked scaled (1 + 2 scaled). Calibration bar, 100 pA, 50 ms.

(D) Summary of the effects of mGluR antagonists on DHPG-LTD compared to interleaved control (Con) experiments. Quantification of the EPSC levels, measured at 30 min following the start of the washout of DHPG and normalized to baseline. *$p < 0.05$ and ***$p < 0.001$.

(E) Example image of a CA1 pyramidal neuron biolistically transfected with SEP-GluA2. Scale bars, 20 μm (left image) and 10 μm (right image).

(F) AMPAR/NMDAR ratios are similar in SEP-GluA2 transfected (n = 8) and neighboring non-transfected (n = 10) neurons. Scale bar, 100 pA, 50 ms. The sample traces on the right show the EPSCs at −70 and +40 mV holding potentials.

(G) Serial recordings of EPSC amplitudes from SEP-GluA2 transfected and non-transfected neurons show similar responses to identical stimulation (n = 10). Average ± SEM response for these neurons (blue).

(H) DHPG-LTD is similar in neurons expressing SEP-GluA2 (n = 6) and in non-transfected neurons (n = 5).

(I) Representative images of SEP-GluA2 fluorescence from control neurons over a 30 min time period and neurons before and 30 min following washout of NMDA (50 μM, 5 min) or DHPG. Scale bar, 5 μm. Arrows point to puncta that decreased in intensity in the DHPG experiment.

(J) Cumulative likelihood distribution of changes of SEP-GluA2 fluorescence in untreated control neurons (813 spines from 15 neurons; black) and neurons treated with NMDA (586 spines from 10 neurons; orange). $p < 0.001$ (K-S test).

(K) Cumulative likelihood distribution of changes in SEP-GluA2 fluorescence in untreated control neurons (560 spines from 9 cells; black) and neurons treated with DHPG (641 spines from 12 cells; purple). $p < 0.001$ (K-S test). Inset: magnified view of the distribution to highlight increases in fluorescence for some DHPG-treated puncta.

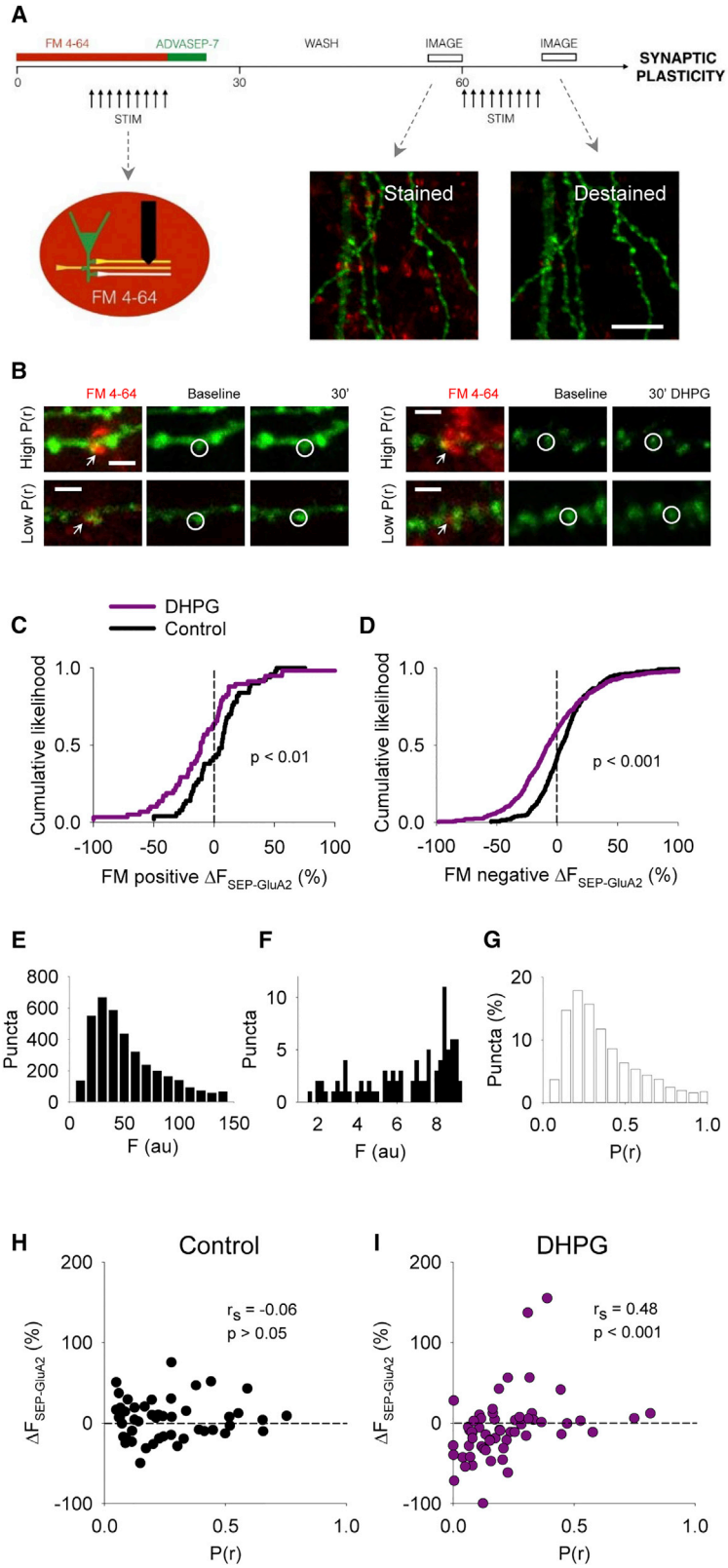

Figure 2. DHPG-Induced AMPAR Trafficking at FM 4-64 Labeled Spines Is Correlated with P(r)

(A) Schematic of the FM staining and destaining protocol (see STAR Methods). FM wash-in is followed by stimulation to the Schaffer collaterals (STIM) to induce vesicular release and subsequent recycling of the plasma membrane to form new stained vesicles. Excess FM not incorporated in new vesicles is removed with ADVASEP-7 followed by 30 min wash. "Stained" image: example image from stratum radiatum of CA1 pyramidal neuron dendrites expressing SEP-GluA2 (green) and presynaptic boutons loaded with FM (red). "De-stained image": image of the same area following de-staining of FM by stimulation of the Schaffer collaterals. Scale bar, 10 μm.

(B) Example images showing SEP-GluA2 expression and FM staining for a control experiment (left) and DHPG experiment (right). Top row: high-P(r) examples. Bottom row: low-P(r) examples. Left: FM and SEP-GluA2 co-staining. Middle: SEP-GluA2 baseline (after destaining). Right: SEP-GluA2 30 min later. Scale bar, 2 μm. Arrows point to example FM puncta; circles highlight adjacent SEP-GluA2 puncta.

(C) Cumulative probability distribution of changes in SEP-GluA2 fluorescence at FM-labeled spines in control neurons (59 spines from 9 neurons; black) and neurons treated with DHPG (58 spines from 8 neurons; purple). $p < 0.01$ (K-S test).

(D) Cumulative probability distribution of changes in SEP-GluA2 fluorescence at FM negative spines in control neurons (490 spines from 9 neurons; black) and neurons treated with DHPG (440 spines from 8 neurons; purple). $p < 0.001$ (K-S test).

(E) Frequency histogram showing the distribution of FM puncta fluorescence intensity with a bin size of 10 arbitrary fluorescence units (au).

(F) Frequency histogram for FM puncta with low fluorescence; bin size 0.3 au.

(G) Histogram showing distribution of P(r) on the basis of FM fluorescence intensity.

(H) Plot of SEP-GluA2 fluorescence changes in untreated neurons over a 30 min time period versus P(r) at individual synapses. In this and (I), r_s and p values indicate results of Spearman's correlation analysis.

(I) Plot of SEP-GluA2 fluorescence changes in synapses 30 min following washout of DHPG versus P(r) at individual synapses.

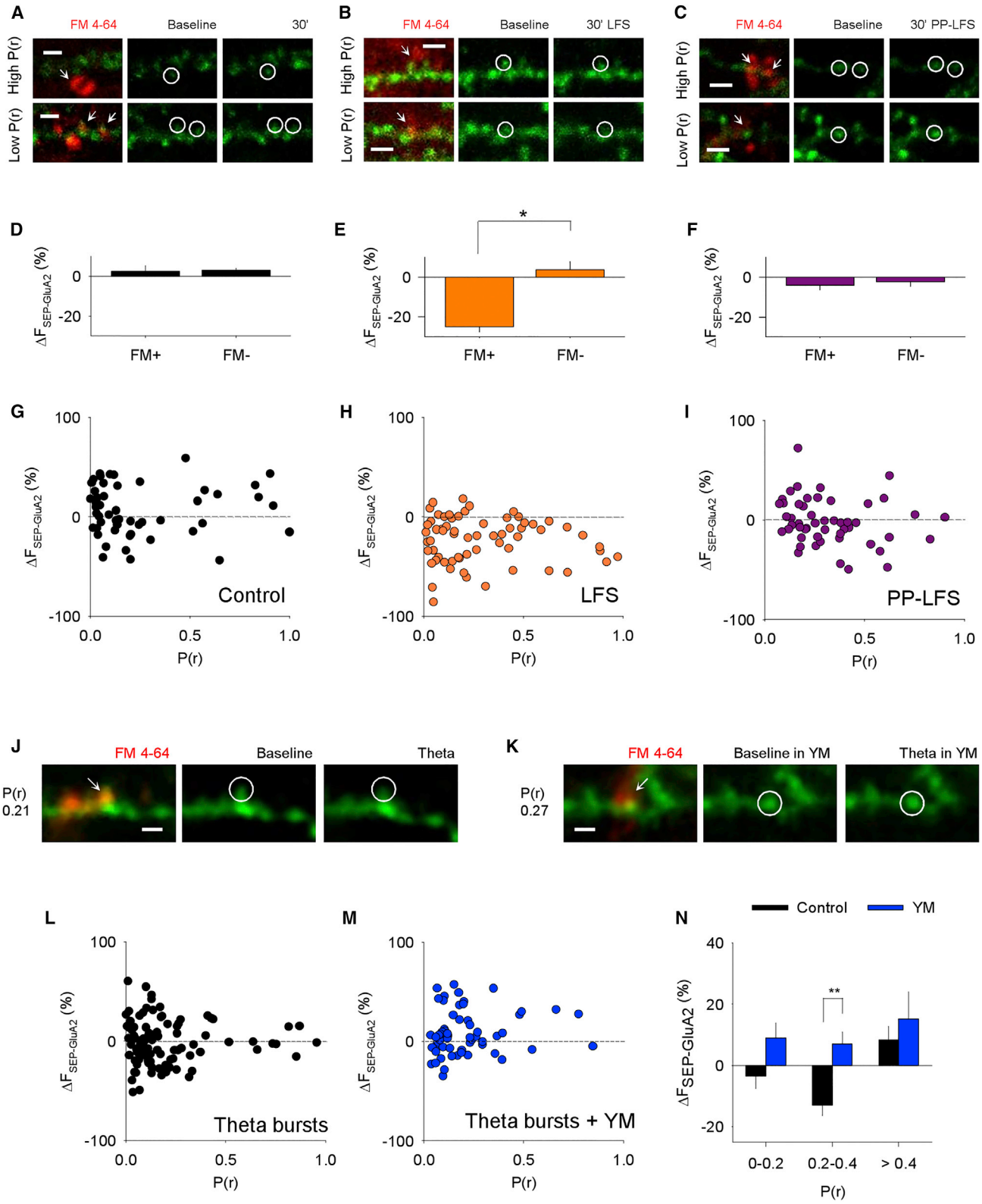

(legend on next page)

To directly test the involvement of P(r) on AMPAR trafficking we altered P(r) by changing the Ca^{2+}/Mg^{2+} ratio from 1 to 4. This resulted in the expected reduction in PPF, from 2.0 ± 0.2 (n = 7) to 1.6 ± 0.2 (n = 7), respectively ($p < 0.05$; Figure S4A). With a ratio of 1, DHPG decreased SEP-GluA2 fluorescence in the majority of puncta as before ($p < 0.01$; Figures S4B and S4C). However, with a ratio of 4, DHPG increased SEP-GluA2 fluorescence relative to untreated controls ($p < 0.001$; Figures S4D and S4E). These results confirm that DHPG-induced AMPAR internalization occurs predominantly at low-P(r) synapses. They further suggest that at high-P(r) synapses, DHPG can increase AMPAR number.

TBS Triggers AMPAR Trafficking that Is Influenced by P(r)

We next examined whether patterns of synaptic stimulation result in AMPAR trafficking that varies with P(r). As before, under control conditions, SEP-GluA2 at both FM-labeled and non-labeled sites was, on average, stable over a 30 min period (3 ± 3% and 3 ± 1%, respectively, $p > 0.05$, n = 6 neurons; Figures 3A and 3D), and individual fluctuations did not correlate with P(r) (Spearman's $r_s = -0.12$, $p > 0.05$, n = 52 synapses from 6 neurons; Figure 3G). In contrast, low-frequency stimulation (LFS) delivered at 1 Hz to enable NMDAR-dependent LTD resulted in a substantial reduction in mean SEP-GluA2 fluorescence (−25 ± 2% of baseline at FM-labeled synapses, n = 6 neurons; Figures 3B and 3E). Consistent with the established input specificity of NMDAR-LTD, the loss of fluorescence was observed only at active synapses, as determined by the co-localization of SEP-GluA2 and FM staining. SEP-GluA2 puncta that were not labeled with FM were stable over the time course of the experiment (4 ± 4%, n = 6, $p < 0.05$; Figures 3B and 3E). At active synapses, there was no relationship between the reduction in SEP-GluA2 and P(r) following LFS (Spearman's $r_s = -0.04$, $p > 0.05$, n = 64 synapses from 6 neurons; Figure 3H). These data demonstrate that NMDAR-LTD, monitored at the level of individual synapses, is input specific and is independent of P(r).

In an attempt to activate mGluRs synaptically, we used paired-pulse LFS (PP-LFS), an established protocol that evokes mGluR-LTD (Huber et al., 2000; Kemp and Bashir, 1999). However, we observed no significant change in SEP fluorescence at either FM-positive or FM-negative sites compared with controls (−4 ± 2% and −2 ± 2%, respectively, n = 8, $p > 0.05$; Figures 3C and 3F). Similarly, there was no correlation with P(r) (Spearman's $r_s = -0.24$, $p > 0.05$, n = 55 synapses from 8 neurons; Figure 3I).

We reasoned that PP-LFS may not be releasing sufficient L-glutamate to activate mGluR1. We therefore examined the effects of TBS (five pulses delivered at 100 Hz, repeated 20 times at 5 Hz), a more physiologically relevant pattern of activation in the hippocampus (Buzsáki, 2002). These experiments were conducted in the presence of L-689,560, to remove the confounding effects that could be associated with NMDAR-dependent forms of synaptic plasticity. We analyzed 94 synapses from 28 neurons (Figures 3J and 3L) and, in interleaved experiments, 59 synapses from 15 neurons in the presence of the mGluR1 antagonist YM (Figures 3K and 3M). We observed a statistically significant reduction in SEP-GluA2 fluorescence at synapses with medium P(r). For example, for a P(r) between 0.2 and 0.4, the fluorescence decreased by 13 ± 3% (21 synapses from 14 neurons; Figures 3J, 3L, and 3N) compared with an increase of 7 ± 4% in the presence of YM (16 synapses from 9 neurons; Figures 3K, 3M, and 3N; $p < 0.01$). Consistent with the effects of DHPG, there was no significant difference between the fluorescence changes when high-P(r) (>0.4) synapses were assessed. However, unlike DHPG-LTD, low-P(r) synapses (<0.2) were unaffected by TBS, presumably because of the lack of sufficient L-glutamate released from these synapses to activate mGluR1. These data show that the synaptic activation of mGluR1 is able to affect AMPAR trafficking and that this is influenced by P(r). The smaller effect, compared with when DHPG was used to activate mGluR1, can be ascribed to the reduced amount of L-glutamate released from the most susceptible low-P(r) synapses.

mGluR1 Is Enriched at Low-P(r) Synapses

Our observations lead to the perplexing question as to why high-P(r) synapses are protected from the effects of DHPG and TBS.

Figure 3. TBS Drives SEP-GluA2 Trafficking at Synapses with Intermediate P(r)

(A) Example images showing SEP-GluA2 expression and FM staining for a control experiment. Top row: high-P(r) examples. Bottom row: low-P(r) examples. Left: FM and SEP-mGluR1 co-staining. Middle: baseline (after destaining). Right: 30 min later. Scale bar, 2 μm. Arrows point to example FM puncta; circles highlight adjacent SEP-mGluR1 puncta.

(B) Example images showing SEP-GluA2 expression and FM staining evaluating the effect of LFS on SEP-GluA2.

(C) Example images showing SEP-GluA2 expression and FM staining assessing the effect of PP-LFS on SEP-GluA2.

(D) Plot of SEP-GluA2 fluorescence changes in spines labeled (FM+) and unlabeled (FM−) with FM over a 30 min period for control conditions (n = 6 neurons). In this and subsequent imaging experiments, the bars represent the mean and the error bars the SEM of n experiments.

(E) Fluorescence changes 30 min following LFS (n = 6 neurons). *$p < 0.05$.

(F) Fluorescence changes 30 min following PP-LFS (n = 8 neurons).

(G) Plot of SEP-GluA2 fluorescence changes in untreated neurons over a 30 min time period versus P(r) at individual synapses (n = 52 synapses from 6 neurons).

(H) Plot of fluorescence changes 30 min following LFS (n = 64 synapses from 6 neurons).

(I) Plot of fluorescence changes 30 min following PP-LFS (n = 55 synapses from 8 neurons).

(J) Example images showing SEP-GluA2 expression and FM staining illustrating the effects of TBS at an intermediate P(r) synapse. Left: FM and SEP-mGluR1 co-staining. Middle: baseline (after destaining). Right: 30 min after TBS. Scale bar, 2 μm. The arrow points to a FM+ punctum; circles highlight the SEP-GluA2 in the corresponding location.

(K) Representative images from an experiment that evaluated of the effects of TBS in YM (2 μM).

(L) Plot of SEP-GluA2 fluorescence changes in neurons following TBS versus P(r) at individual synapses (94 synapses from 28 neurons).

(M) Plot of P(r) relationship with SEP-GluA2 fluorescence changes following TBS in YM (59 synapses from 15 neurons).

(N) Average changes in SEP-GluA2 fluorescence with respect to P(r) due to TBS (black bars) and TBS applied in YM (blue bars), grouped according to P(r). **$p < 0.01$.

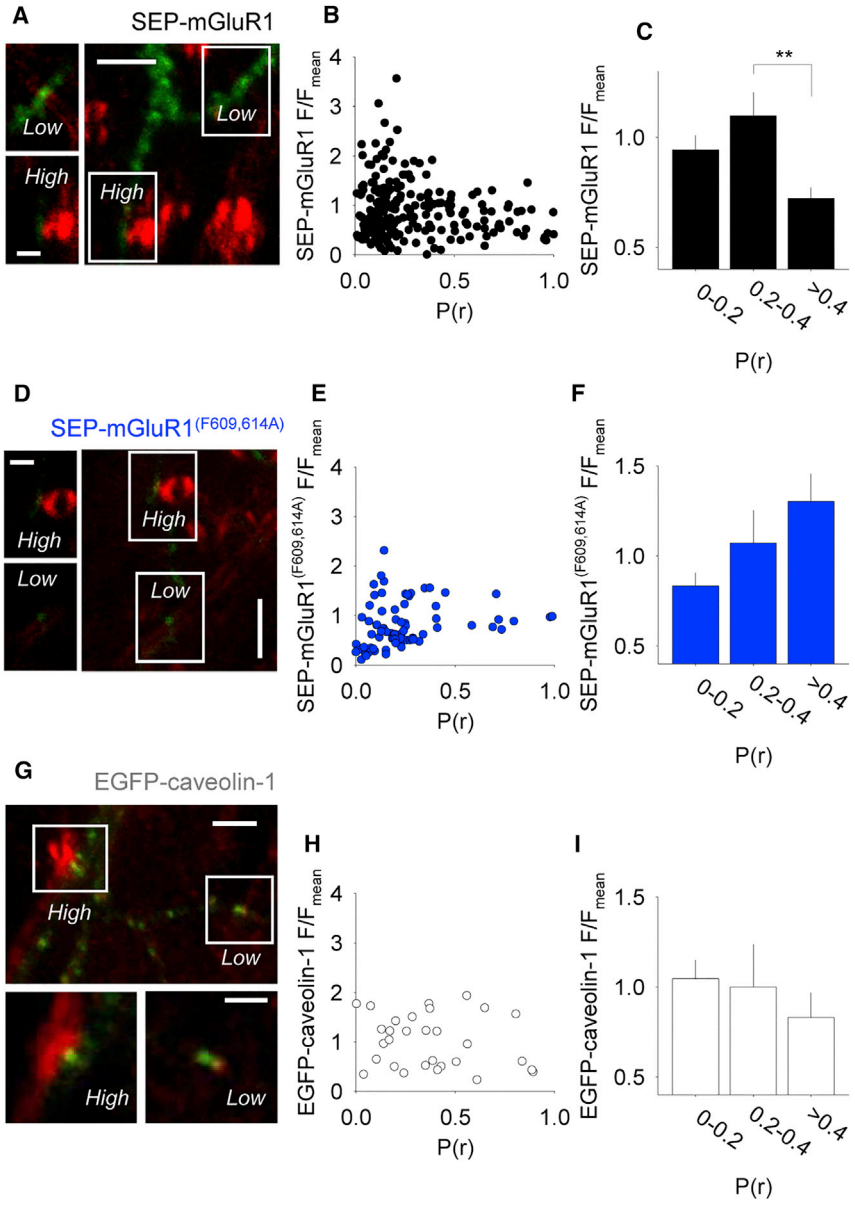

Figure 4. SEP-mGluR1 Is Reduced at High-P(r) Synapses

(A) Example fluorescence images showing SEP-mGluR1 expression (green) and FM staining (red). Main image: z projection; insets: individual z plane image. "Low" and "high" refer to P(r). Scale bars, 5 μm (main image) and 2 μm (individual z-plane images).

(B) Plot of SEP-mGluR1 fluorescence and P(r) at individual synapses (229 synapses from 42 neurons). In this and subsequent charts values normalized to the average fluorescence of FM-labeled spines (F/F_{mean}).

(C) Average SEP-mGluR1 fluorescence binned according to P(r). **$p < 0.01$.

(D) Example images showing SEP-mGluR1(F609, 614A) expression and FM staining.

(E) Plot of SEP-mGluR1(F609,614A) and P(r) at individual synapses (75 synapses from 9 neurons).

(F) Average SEP-mGluR1(F609,614A) fluorescence binned according to P(r).

(G) Example images comparing EGFP-caveolin-1 fluorescence (green) and FM staining (red). Scale bars, 10 μm (main image) and 5 μm (insets).

(H) Plot of EGFP-caveolin-1 fluorescence and P(r) at individual synapses (30 synapses from 4 neurons).

(I) Average EGFP-caveolin-1 fluorescence binned according to P(r).

We initially questioned whether the distribution of mGluR1 was similarly correlated with P(r). Therefore, we expressed SEP-mGluR1 and measured P(r) using FM as before. SEP-mGluR1 fluorescence was visible in spines and also in areas of the dendritic shaft (Figure 4A), which is consistent with reports that group I mGluRs are found in peri-synaptic and extra-synaptic sites (Luján et al., 1997). We found that mGluR1 is enriched at medium-P(r) synapses (0.2–0.4) compared with high-P(r) synapses (>0.4): 1.1 ± 0.1 versus 0.72 ± 0.05, respectively ($p < 0.01$, n = 229 synapses from 41 neurons; Figures 4B and 4C).

We wondered whether the differential distribution of mGluR1 at synapses could be produced by regulation of its internalization from the plasma membrane. It is known that caveolin-1 binds directly to mGluR1 and can organize proteins at membrane locations (Francesconi et al., 2009; Hong et al., 2009; Roh et al., 2014). If two crucial phenylalanine residues, 609 and 614, in mGluR1 are mutated, then binding to caveolin-1 is disrupted and mGluR1 internalization is reduced. Accordingly, we expressed SEP-mGluR1(F609, 614A) (Hong et al., 2009) and observed no statistically significant difference in its distribution at medium- and high-P(r) synapses (1.1 ± 0.2 and 1.3 ± 0.2, respectively, $p > 0.05$, n = 75 synapses from 9 neurons; Figures 4D–4F). Thus, the differential distribution of mGluR1 at synapses likely involves a caveolin-1:mGluR1 interaction.

We considered the possibility that caveolin-1 distribution at synapses is regulated by P(r). To examine this we used EGFP-caveolin-1 but did not observe any differential expression of EGFP-caveolin-1 with respect to P(r). Normalized EGFP-caveolin-1 fluorescence was 1.0 ± 0.2 and 0.8 ± 0.1 at medium- and high-P(r) synapses, respectively ($p > 0.05$, n = 30 synapses from 4 neurons; Figures 4G–4I). Thus, the effect of P(r) on mGluR1 synaptic localization cannot be attributed to a differential distribution of caveolin-1 per se. Rather, these observations suggest that caveolin-1-dependent internalization of mGluR1 is influenced by P(r) via some other mechanism.

Activity-Dependent Trafficking of mGluR1 at Synapses

We next considered the possibility that mGluR1 levels are regulated by activity, such that glutamate release from high-P(r) synapses results in a lower level of surface mGluR1. Although agonist-induced internalization of mGluR1 occurs in

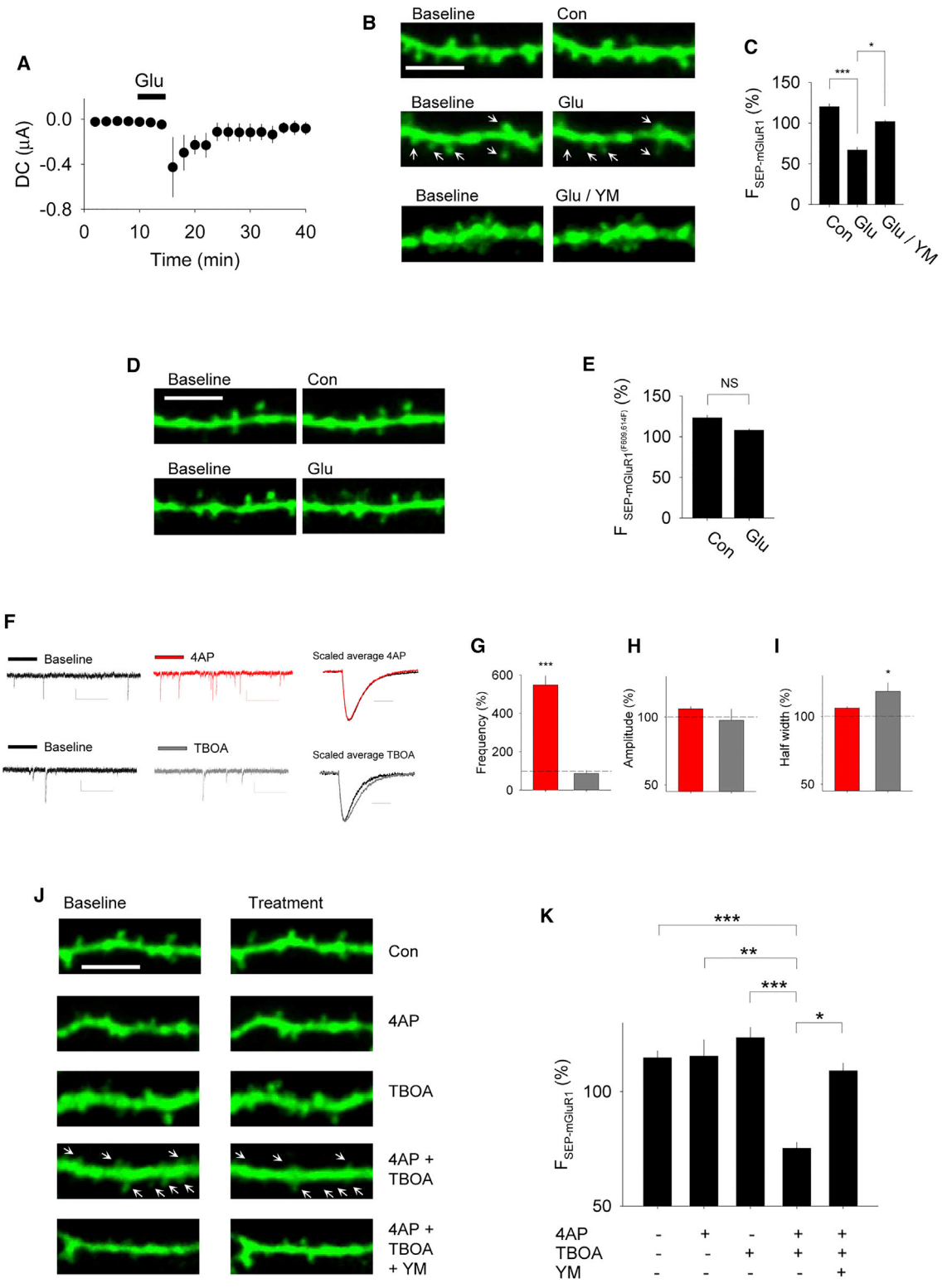

Figure 5. Glutamate Induces SEP-mGluR1 Internalization

(A) Summary data showing effect of 300 μM L-glutamate (Glu) on holding currents in pyramidal neurons (n = 4).

(B) Example images showing the effects of Glu on SEP-mGluR1 applied alone or in combination with YM (2 μM). Scale bar, 5 μm.

(legend continued on next page)

heterologous expression systems (Doherty et al., 1999), it is unknown whether synaptically expressed mGluR1 is subject to such regulation. First, we tested the effects of L-glutamate at a concentration (300 μM, 5 min) that induced an inward current in CA1 neurons (n = 4; Figure 5A). Under control conditions, the fluorescence of both SEP-mGluR1 and SEP-mGluR1(F609,614A) were stable over time, displaying similar, statistically non-significant, increases (120 ± 2, n = 12, and 123 ± 3%, n = 9, respectively, after 15 min of imaging; Figures 5B–5E). L-glutamate resulted in a rapid reduction in SEP-mGluR1 fluorescence (68 ± 3%, n = 9), which was prevented by the mGluR1 antagonist YM (102 ± 2%, $p < 0.05$, n = 7; Figures 5B and 5C). In contrast, L-glutamate had no effect on cells expressing the SEP-mGluR1(F609,614A) construct (108 ± 2%, n = 7; Figures 5D and 5E). This demonstrates that L-glutamate can rapidly induce caveolin-1-dependent internalization of mGluR1 in neurons.

To investigate whether endogenously released glutamate has a similar effect on SEP-mGluR1, we applied the potassium channel antagonist 4-aminopyridine (4-AP; 200 μM) to enhance release and/or the excitatory amino acid transporter (EAAT) inhibitor threo-β benzyloxyaspartic acid (TBOA; 10 μM) to enhance spillover of neurotransmitter. As expected, 4-AP treatment increased spontaneous excitatory postsynaptic current (sEPSC) frequency (to 547 ± 48% of baseline, n = 7, $p < 0.001$; Figures 5F and 5G) and TBOA treatment increased sEPSC duration (half-width increased to 118 ± 7% of baseline, n = 7, $p < 0.05$; Figures 5F and 5I). Neither treatment resulted in a change in the sEPSC amplitude (106 ± 2 and 98 ± 8, respectively, $p > 0.05$; Figures 4F and 4H).

Neither the 4-AP nor TBOA treatments, when applied alone, affected SEP-mGluR1 fluorescence. Following 30 min treatment with 4-AP or TBOA, fluorescence was 115 ± 7% (n = 8) and 124 ± 4% (n = 7), respectively, compared with fluorescence in untreated neurons of 115 ± 3% (n = 11, $p > 0.05$, Figures 5J and 5K). However, when these treatments were combined, SEP-mGluR1 fluorescence decreased to 75 ± 3% (n = 7, $p < 0.001$; Figures 5J and 5K). The findings suggest that an increase in the frequency of L-glutamate release is insufficient to regulate mGluR1 levels unless spillover occurs, consistent with the need to activate peri-synaptic or extra-synaptic mGluRs. The effect of the combined treatment was blocked by YM (109 ± 3%, n = 6, $p < 0.01$; Figures 5J and 5K), consistent with the regulation being dependent on activation of mGluR1. Thus, endogenous release of L-glutamate, onto extra-synaptic or peri-synaptic mGluR1 receptors, can regulate the surface levels of mGluR1.

Theta Burst Triggers mGluR1 Trafficking that Correlates with P(r)

Because TBS was able to regulate SEP-GluA2 localization in an mGluR1-dependent manner, we reasoned that TBS may affect the surface levels of mGluR1. Consistent with this idea, TBS triggered a reduction in SEP-mGluR1 fluorescence, and the magnitude of this effect correlated with P(r) (Spearman's $r_s = -0.31$, $p < 0.01$, n = 86 synapses from 20 neurons; Figures 6B and 6E). Furthermore, there was no net reduction in SEP-mGluR1 and no correlation with P(r) in either control (i.e., non-stimulated) neurons (Spearman's $r_s = -0.05$, $p > 0.05$, n = 42 synapses from 11 neurons; Figures 6A and 6D) or where the TBS was applied in the presence of YM (Spearman's $r_s = 0.07$, $p > 0.05$, n = 43 synapses from 10 neurons; Figures 6C and 6F). When changes in SEP-mGluR1 fluorescence at high- and low-P(r) synapses were compared, theta bursts resulted in a selective effect at high-P(r) synapses (−13 ± 1% and 4 ± 1%, respectively; Figure 6H), whereas there was no significant difference between high- and low-P(r) synapses either under control conditions (8 ± 2% and 6 ± 2%, respectively; Figure 6G) or when theta bursts were applied in the presence of YM (2 ± 3% and 0 ± 2%, respectively; Figure 6I). In conclusion, there is an activity-dependent reduction of surface mGluR1 at high-P(r) synapses. This process is sufficient to account for the effects of P(r) on AMPAR trafficking. Consequently, the activity-dependent regulation of mGluR1 pre-tunes the susceptibility of synapses to postsynaptic weakening according to their P(r).

DISCUSSION

In the present study we have, for the first time, identified a relationship between the extent of postsynaptic AMPAR trafficking and the P(r) of a synapse. We found less AMPAR trafficking at higher P(r) synapses when mGluR1 was activated pharmacologically, using DHPG, or synaptically, using TBS. The underlying mechanism is an activity-dependent reduction in the levels of surface mGluR1, which then protects high-P(r) synapses from synaptic weakening. Thus, the susceptibility of synapses to postsynaptic weakening is related to their P(r), through a mechanism governed by mGluR1. These new findings are shown schematically in Figure 7.

(C) Quantification of effects of Glu on SEP-mGluR1. Mean ± SEM changes for control neurons (n = 12), neurons treated with Glu (n = 9), and neurons treated with Glu in the presence of YM (n = 7). *$p < 0.05$, ***$p < 0.001$.

(D) Example images showing the effects of Glu on SEP-mGluR1(F609,614A) expressing neurons. Scale bar, 5 μm.

(E) Quantification of effects of Glu on SEP-mGluR1(F609,614A) expressing neurons. Mean ± SEM changes for control neurons (n = 9) and Glu-treated neurons (n = 7).

(F) Example traces showing effects of 200 μM 4-AP (red) and 10 μM TBOA (gray) on sEPSC frequency and half-width. Scale bars, 20 pA, 0.5 s (traces in first two columns) and 10 ms (right-hand column traces).

(G) Summary data showing effects of 4-AP (red bars; n = 7) and TBOA (gray bars; n = 7) on sEPSC frequency as a percentage of baseline. ***$p < 0.001$.

(H) Summary data for sEPSC amplitudes.

(I) Summary data for sEPSC half-widths. *$p < 0.05$.

(J) Example images showing effects of 4-AP and TBOA on SEP-mGluR1 fluorescence applied alone, in combination, and together with YM (2 μM). Scale bar, 5 μm.

(K) Summary data showing effect on SEP-mGluR1 fluorescence of 4-AP alone (n = 8), TBOA alone (n = 7), 4-AP and TBOA in combination (n = 7) and 4-AP plus TBOA in combination with YM (2 μM; n = 6). *$p < 0.05$, **$p < 0.01$, and ***$p < 0.001$.

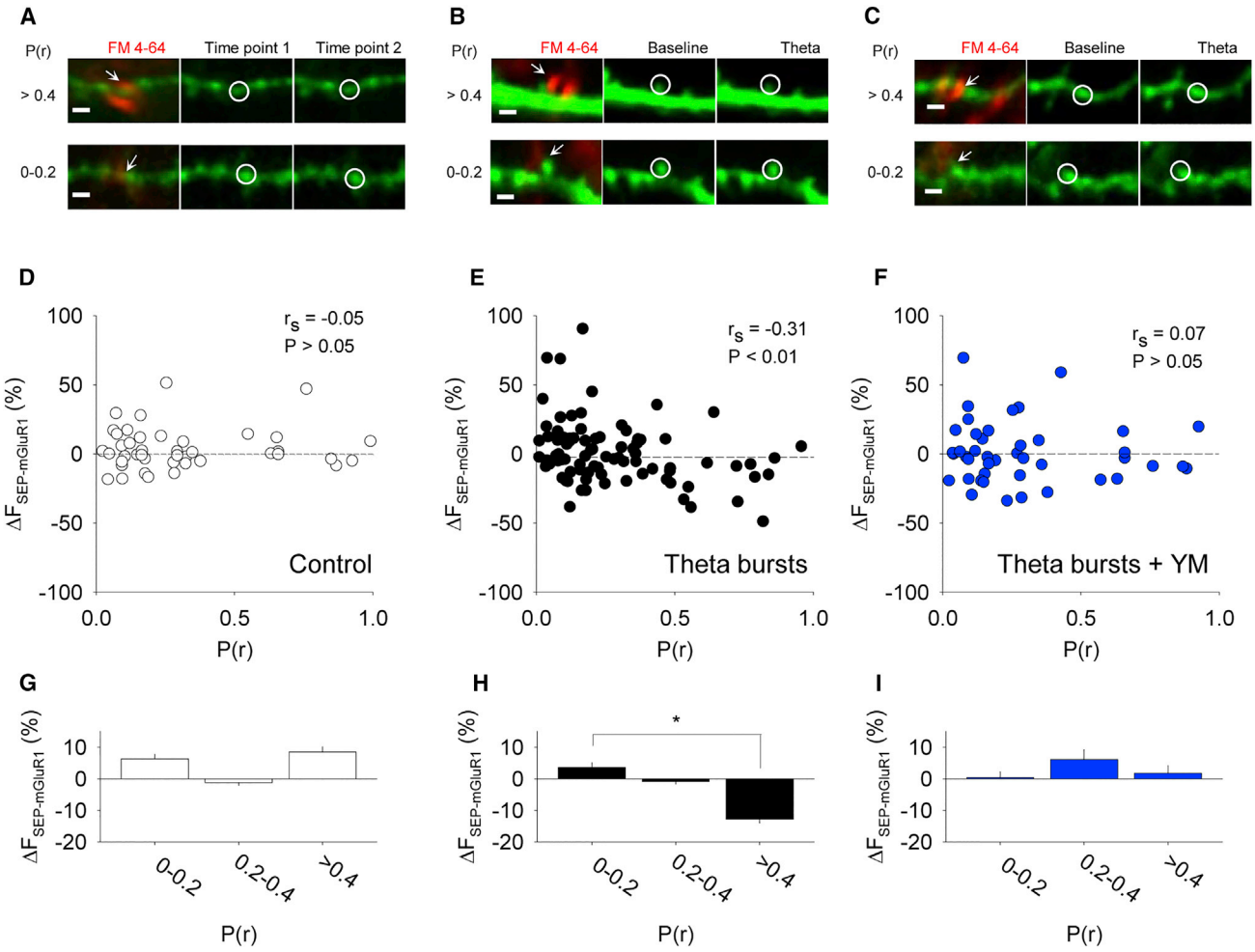

Figure 6. TBS Causes SEP-mGluR1 Trafficking at High-P(r) Synapses

(A) Example images showing SEP-mGluR1 expression and FM staining for a control experiment. Top row: high-P(r) examples. Bottom row: low-P(r) examples. Left: FM and SEP-mGluR1 co-staining. Middle: baseline (after destaining). Right: 30 min later. Scale bar, 2 μm. Arrows point to example FM puncta; circles highlight adjacent SEP-mGluR1 puncta.

(B) Corresponding images showing the effect of TBS.

(C) Corresponding images showing the effect of TBS in YM.

(D) Plot of SEP-mGluR1 fluorescence changes in untreated neurons versus P(r) at individual synapses (42 synapses from 11 neurons). r_s and p values are from a Spearman's correlation analysis.

(E) SEP-mGluR1 versus P(r) plot immediately following TBS (86 synapses from 20 neurons).

(F) SEP-mGluR1 versus (Pr) plot immediately following TBS in YM (43 synapses from 10 neurons).

(G) Average change in SEP-mGluR1 fluorescence binned by P(r), in control neurons.

(H) Corresponding analysis for TBS. *p < 0.05

(I) Corresponding analysis for TBS in YM.

A Postsynaptic Form of DHPG-LTD Triggered by Activation of mGluR1

Multiple forms of DHPG-LTD have been described that differ in their locus of expression and in the group I mGluR subtype that triggers their induction (reviewed in Gladding et al., 2009). The type of DHPG-LTD studied here at CA1 synapses in organotypic slices is mediated exclusively by postsynaptic alterations, as determined by the lack of any change in PPF, and is triggered exclusively by the activation of mGluR1 (see also Nadif Kasri et al., 2011). DHPG-LTD has been shown to require synaptic stimulation (Scholz et al., 2010), but consistent with a previous report (Fitzjohn et al., 1999), we found that the necessary activation could be provided by a heterosynaptic input.

The Use of SEP and FM for Assessing Synaptic Function

The development of pH-sensitive GFP derivatives has greatly facilitated the study of secretion events (Miesenböck et al., 1998). We adopted this method for the study of AMPAR trafficking (Ashby et al., 2004) and this has since been used to advance our understanding of how AMPAR trafficking contributes to synaptic plasticity (reviewed in Roth et al., 2017). It has previously been established that alterations in fluorescence of

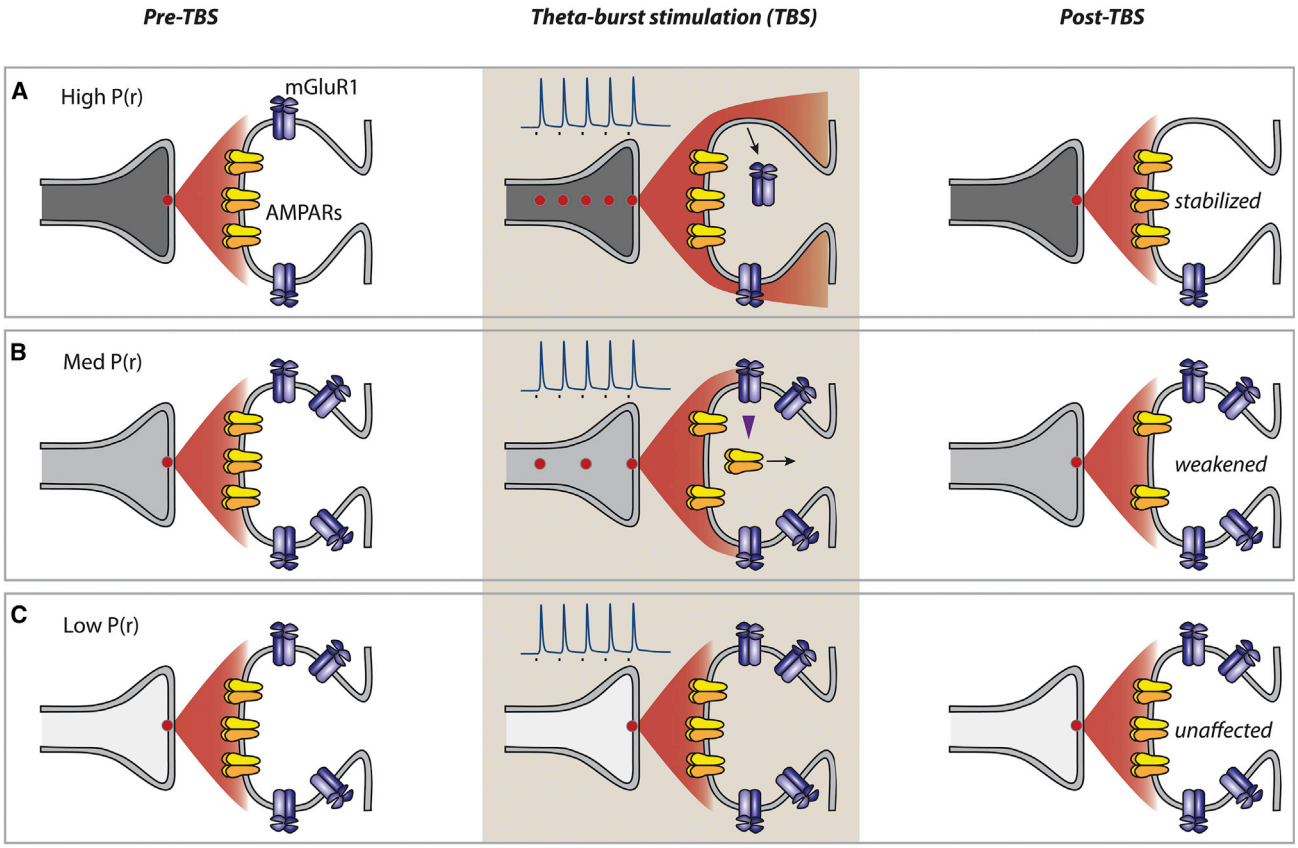

Figure 7. Schematic Representation of Synaptic Glutamate Receptor Trafficking as a Function of P(r)

(A) High-P(r) synapses. There is less mGluR1, because of agonist-induced internalization, under baseline conditions (left). During TBS there is sufficient L-glutamate released to drive internalization of some residual mGluR1, but there is insufficient mGluR1 to drive AMPAR trafficking (center). The loss of mGluR1 further stabilizes high-P(r) synapses, by protecting them from mGluR1-dependent synaptic weakening (right).

(B) Medium-P(r) synapses. During TBS, there is insufficient L-glutamate to rapidly drive internalization of mGluR1 but sufficient to activate mGluR1 to drive AMPAR trafficking (most probably lateral diffusion followed by endocytosis). This results in a weakened synapse and one that is still susceptible to additional mGluR1-driven synaptic weakening.

(C) Low-P(r) synapses experience insufficient L-glutamate during TBS for there to be any effects on either mGluR1 surface levels or mGluR1-driven AMPAR trafficking.

these constructs accurately reflects changes in AMPAR surface expression at spines (Ashby et al., 2004; Rathje et al., 2013; Wilkinson et al., 2014). GluA2 undergoes Q-R RNA editing at residue 607, resulting in a more restricted trafficking of GluA2 containing AMPARs to the cell surface (Greger et al., 2002). In line with previous studies (Kopec et al., 2006; Hsieh et al., 2006; Araki et al., 2010; Granger et al., 2013), we expressed an unedited version of GluA2 (Figure 1E), since SEP-GluA2(R) expression levels were too low to obtain an adequate signal-to-noise ratio (see STAR Methods). Although the expression of SEP-GluA2(Q) may increase the Ca^{2+} permeability of synapses, this did not interfere with the ability of DHPG to induce LTD, with identical levels being observed in transfected and non-transfected neurons. Notably, unlike most other forms of synaptic plasticity, DHPG-LTD is not dependent on Ca^{2+} levels in hippocampal neurons (Fitzjohn et al., 2001; Schnabel et al., 1999).

Since their introduction for the study of vesicle recycling at the neuromuscular junction (Betz and Bewick, 1992) and the hippocampus (Ryan et al., 1993), FM dyes have been used extensively to monitor presynaptic fusion events (Branco and Staras, 2009). The subsequent development of agents that can reduce background staining of FM dyes has facilitated their use in brain-slice preparations (Kay et al., 1999; Pyle et al., 1999). Here we have combined SEP tagged glutamate receptors and FM imaging to examine, for the first time, the relationship between glutamate receptor trafficking and P(r) at individual synapses. As a test of the validity of the combined SEP and FM imaging approach we studied synaptically induced NMDAR-LTD, a process that is known to be input specific (Daw et al., 2002; Dudek and Bear, 1992). Consistent with this property, we found a pronounced loss of synaptic SEP-GluA2 at FM-positive but no change at FM-negative sites. This verifies, in the most direct manner possible, that SEP-GluA2 is reflecting AMPAR trafficking during synaptic plasticity events.

LTD and AMPAR Trafficking

The observation that DHPG-LTD led to a synaptic loss of SEP-GluA2 is consistent with previous work that has used antibodies

that recognize extracellular epitopes on living neurons (Richmond et al., 1996) to study native AMPAR trafficking (Moult et al., 2006; Snyder et al., 2001; Xiao et al., 2001). We found that DHPG caused a reduction in SEP-GluA2 fluorescence in a subset of synapses, an observation that is consistent with previous observations of native AMPARs labeled with antibodies (Xiao et al., 2001). We also observed a greater variation in the distribution of SEP-GluA2 after DHPG treatment, which is consistent with our previous work in dissociated cell culture (Sanderson et al., 2011). In this earlier study we observed no net decrease in intensity at SEP-GluA2 puncta in dissociated hippocampal neurons studied in the presence of TTX (Sanderson et al., 2011). This difference can be explained by the requirement for synaptic activation to observe a net internalization of AMPARs (Figure S2). The relatively small reductions in SEP-GluA2 fluorescence was not due to a problem with detection, because in interleaved experiments we observed substantial reductions in SEP-GluA2 fluorescence when neurons were treated with NMDA. The effects of NMDA were similar to our previous work (Ashby et al., 2004; Sanderson et al., 2011) in which NMDA induced a pronounced loss of spine fluorescence, which may be attributed to the rapid endocytosis at peri-synaptic and/or extra-synaptic sites, followed by lateral diffusion of synaptic GluA2 away from the synapse to fill the vacated non-synaptic sites (Ashby et al., 2004; Roth et al., 2017). Consistent with SEP-GluA2 providing an accurate measure of endogenous trafficking, NMDA treatment has been shown to rapidly lead to AMPAR endocytosis when assessed using antibodies directed to native receptors (Beattie et al., 2000; Casimiro et al., 2011; Ehlers, 2000; Fiuza et al., 2017; Moult et al., 2006).

AMPAR Trafficking Is Affected by P(r)

By comparing the extent of AMPAR trafficking with P(r) at individual synapses, we made the surprising observation that these parameters are interrelated when DHPG is used to trigger plasticity. Specifically, the ability of DHPG to reduce SEP-GluA2 expression was inversely correlated with the P(r) of the synapses. One consequence of this relationship is that activation of mGluR1 will selectively remove AMPARs from low-P(r) synapses resulting in a residual response that has a greater contribution from high-P(r) synapses. We found that the ability of DHPG to affect SEP-GluA2 trafficking not only correlated with P(r) but was dramatically affected when P(r) was altered by changing the Ca^{2+}:Mg^{2+} ratio (Figure S4). Although interpretation of these results may be complicated by changes in postsynaptic Ca^{2+} signaling it is relevant to note that DHPG-LTD in the hippocampus is independent of postsynaptic Ca^{2+} (Schnabel et al., 1999; Fitzjohn et al., 2001). Therefore, we consider that it is most likely that these alterations in DHPG-induced AMPAR trafficking are due to the changes to P(r). Thus, increasing P(r) converted the effects of DHPG from predominantly a decrease in puncta fluorescence to an increase in puncta fluorescence. This result is consistent with reports that in acute slices the magnitude of mGluR-LTD is sensitive to changes in the Ca^{2+} to Mg^{2+} ratio (Oliet et al., 1997; Watabe et al., 2002). Collectively, these experiments have uncovered an unexpected relationship between mGluR1 activation and AMPAR trafficking that depends upon the P(r) level of a given synapse.

Mechanisms for Reduced AMPAR Trafficking at High-P(r) Synapses

The finding that mGluR1 was preferentially internalized at high-P(r) synapses may account for the reduced trafficking of AMPARs at these synapses in response to DHPG or TBS. The resultant lower expression levels of mGluR1 at high-P(r) synapses effectively protects them from postsynaptic weakening. It implies that the signaling is highly localized, such that mGluR1 activation on or near a spine regulates AMPAR trafficking exclusively or predominantly at that same spine. We found that (1) application of L-glutamate, (2) enhanced spontaneous L-glutamate release, or (3) TBS could promote SEP-mGluR1 synaptic removal. The lower levels of SEP-mGluR1 at higher P(r) synapses can, therefore, be explained by the more frequent release of L-glutamate. We found that increasing synaptic activity with 4-AP was not sufficient to induce SEP-mGluR1 trafficking but that inhibition of the EAATs was also necessary. This is consistent with the need for L-glutamate to "spill over" to peri-synaptically or extra-synaptically located mGluRs. Under a variety of conditions, increased activity results in glutamate spillover that can activate peri-synaptic or extra-synaptic receptors (Arnth-Jensen et al., 2002; Hires et al., 2008; Lozovaya et al., 1999). Our finding that TBS, a pattern of stimulation readily observed *in vivo* (Buzsáki, 2002), was effective at driving internalization of mGluR1 suggests that this mechanism is engaged physiologically.

The molecular mechanism by which glutamate leads to the removal of mGluRs at synapses is only partially understood. In HEK cells, mGluR1 is internalized in response to L-glutamate through an arrestin- and clathrin-dependent mechanism (Pula et al., 2004). We found that for P(r) to influence mGluR1 removal, it requires an interaction between the receptor and caveolin-1, a protein known to regulate mGluR1 trafficking and function (Francesconi et al., 2009; Hong et al., 2009; Roh et al., 2014; Takayasu et al., 2010). However, the distribution of caveolin-1 was independent of P(r), indicating that this protein does not dictate the relationship between P(r) and postsynaptic AMPAR trafficking. Arc/Arg3.1 is required for DHPG-LTD (Waung et al., 2008) and is preferentially trafficked to artificially inactivated synapses through a process termed inverse synaptic tagging (Okuno et al., 2012), so Arc/Arg3.1 may therefore contribute to the inverse relationship described here.

Functional Significance of Linking AMPAR Internalization to P(r)

What is the purpose of a mechanism designed to remove AMPARs as a function of P(r)? Potentially one role could be to preserve synapses that are more active presynaptically at the expense of less active synapses. It has been shown that pre- and postsynaptic function is correlated (Hardingham et al., 2010; Kay et al., 2011; Thiagarajan et al., 2005; Tokuoka and Goda, 2008), via unknown processes that emerge during development (Kay et al., 2011) and in response to enhanced neuronal activity (Tokuoka and Goda, 2008). This relationship is maintained during the enhancement of synaptic transmission induced by chronic AMPAR blockade (Thiagarajan et al., 2005). Previous work linking pre- and postsynaptic function has focused on retrograde messengers, for example BDNF and other transsynaptic signaling molecules (Henry et al., 2012; Jakawich et al.,

2010; Lindskog et al., 2010; Williams et al., 1989; Zhuo et al., 1993). Our findings provide another potential mechanism by which this relationship may be generated, as a selective preservation of postsynaptic AMPARs at high-P(r) synapses would lead to such a correlation.

In the present study we blocked NMDARs to remove confounding factors that might be associated with NMDAR-dependent plasticity. In the physiological setting, the mGluR1-driven changes will, of course, exist alongside other forms of synaptic plasticity. During development, theta activity develops (Charlesworth et al., 2015; Kim et al., 2016) and will enable NMDAR-dependent LTP. The finding that TBS can also drive a reduction in postsynaptic mGluR1 implies that synapses that undergo LTP will be protected against mGluR1-driven synaptic weakening. This mechanism could therefore contribute to the activity-dependent refinement of neural circuits during development. The linking of P(r) with AMPAR trafficking may be particularly relevant early in development, when LTP involves changes both in P(r) and in AMPAR trafficking (Palmer et al., 2004). However, mGluR1 has been found to play a role in LTD later in development in the hippocampus (Hou and Klann, 2004; Volk et al., 2006) and the parallel pathway in the cerebellum (Aiba et al., 1994; Conquet et al., 1994). It will be interesting to determine whether mGluR1 serves a similar function at these and other synapses in the CNS and at different developmental time points.

Conclusions

We have described a link between the P(r) of a synapse and the degree of AMPAR removal during a form of LTD triggered by the activation of mGluR1. We show that the underlying mechanism is the activity-dependent synaptic removal of mGluR1 and that this can be triggered by TBS. The consequence of this process is that the lower expression levels of mGluR1 at high-P(r) synapses protects them from postsynaptic weakening. More generally, postsynaptic plasticity at glutamatergic synapses can be pre-tuned by the presynaptic strength of the synapse.

STAR★METHODS

Detailed methods are provided in the online version of this paper and include the following:

- KEY RESOURCES TABLE
- CONTACT FOR REAGENT AND RESOURCE SHARING
- EXPERIMENTAL MODEL AND SUBJECT DETAILS
  - Preparation of organotypic culture
- METHOD DETAILS
  - Biolistic transfection
  - Patch clamp electrophysiology
  - EGFP and SEP imaging
  - FM4-64 imaging
- QUANTIFICATION AND STATISTICAL ANALYSIS
- DATA AND SOFTWARE AVAILABILITY

SUPPLEMENTAL INFORMATION

Supplemental Information includes four figures and can be found with this article online at https://doi.org/10.1016/j.celrep.2018.12.010.

ACKNOWLEDGMENTS

This study was supported by the World-Class University (WCU) program through the National Research Foundation of Korea (R32-10142), a National Research Foundation of Korea (NRF) grant funded by the Korean government (Ministry of Science, ICT and Future Planning [MSIP]) (2018R1A5A2025964), U.K. Medical Research Council (MRC) grant MR/K023098/1, Biotechnology and Biological Sciences Research Council (BBSRC) grant BB/K019899/1, European Union (EU) grant 341089-HippoKAR, and Canadian Institutes of Health Research (CIHR) Foundation grant 154276. This work was also supported by the Brain Canada Foundation through the Canada Brain Research Fund, with the financial support of Health Canada.

AUTHOR CONTRIBUTIONS

T.M.S. performed and analyzed all experiments, prepared some of the SEP-GluA2 constructs, and edited the manuscript. Y.H.H. prepared the SEP-mGluR1 constructs. A.N.N. assisted with some of the imaging analysis. J.G. constructed the scheme and edited the manuscript. C.A.B. prepared the SEP-GluA2 constructs and edited the manuscript. Y.L., H.-D.K., and G.H.S. prepared the SEP-GluA2 constructs. M.A. contributed expertise to the electrophysiological experiments. M.Z., K.K., B.-K.K., and S.J.K. helped conceive and supervised the project. G.L.C. conceived and supervised the project, wrote the first version of the manuscript, and edited subsequent versions.

DECLARATION OF INTERESTS

The authors declare no competing interests.

Received: January 16, 2018
Revised: September 28, 2018
Accepted: December 3, 2018
Published: December 26, 2018

REFERENCES

Aiba, A., Kano, M., Chen, C., Stanton, M.E., Fox, G.D., Herrup, K., Zwingman, T.A., and Tonegawa, S. (1994). Deficient cerebellar long-term depression and impaired motor learning in mGluR1 mutant mice. Cell *79*, 377–388.

Anderson, W.W., and Collingridge, G.L. (2007). Capabilities of the WinLTP data acquisition program extending beyond basic LTP experimental functions. J. Neurosci. Methods *162*, 346–356.

Anderson, W.W., Fitzjohn, S.M., and Collingridge, G.L. (2012). Automated multi-slice extracellular and patch-clamp experiments using the WinLTP data acquisition system with automated perfusion control. J. Neurosci. Methods *207*, 148–160.

Araki, Y., Lin, D.T., and Huganir, R.L. (2010). Plasma membrane insertion of the AMPA receptor GluA2 subunit is regulated by NSF binding and Q/R editing of the ion pore. Proc. Natl. Acad. Sci. U S A *107*, 11080–11085.

Arnth-Jensen, N., Jabaudon, D., and Scanziani, M. (2002). Cooperation between independent hippocampal synapses is controlled by glutamate uptake. Nat. Neurosci. *5*, 325–331.

Ashby, M.C., De La Rue, S.A., Ralph, G.S., Uney, J., Collingridge, G.L., and Henley, J.M. (2004). Removal of AMPA receptors (AMPARs) from synapses is preceded by transient endocytosis of extrasynaptic AMPARs. J. Neurosci. *24*, 5172–5176.

Ashby, M.C., Maier, S.R., Nishimune, A., and Henley, J.M. (2006). Lateral diffusion drives constitutive exchange of AMPA receptors at dendritic spines and is regulated by spine morphology. J. Neurosci. *26*, 7046–7055.

Auerbach, B.D., Osterweil, E.K., and Bear, M.F. (2011). Mutations causing syndromic autism define an axis of synaptic pathophysiology. Nature *480*, 63–68.

Bear, M.F., Huber, K.M., and Warren, S.T. (2004). The mGluR theory of fragile X mental retardation. Trends Neurosci. *27*, 370–377.

Beattie, E.C., Carroll, R.C., Yu, X., Morishita, W., Yasuda, H., von Zastrow, M., and Malenka, R.C. (2000). Regulation of AMPA receptor endocytosis by a signaling mechanism shared with LTD. Nat. Neurosci. *3*, 1291–1300.

Betz, W.J., and Bewick, G.S. (1992). Optical analysis of synaptic vesicle recycling at the frog neuromuscular junction. Science *255*, 200–203.

Branco, T., and Staras, K. (2009). The probability of neurotransmitter release: variability and feedback control at single synapses. Nat. Rev. Neurosci. *10*, 373–383.

Bredt, D.S., and Nicoll, R.A. (2003). AMPA receptor trafficking at excitatory synapses. Neuron *40*, 361–379.

Buzsáki, G. (2002). Theta oscillations in the hippocampus. Neuron *33*, 325–340.

Casimiro, T.M., Sossa, K.G., Uzunova, G., Beattie, J.B., Marsden, K.C., and Carroll, R.C. (2011). mGluR and NMDAR activation internalize distinct populations of AMPARs. Mol. Cell. Neurosci. *48*, 161–170.

Charlesworth, P., Cotterill, E., Morton, A., Grant, S.G., and Eglen, S.J. (2015). Quantitative differences in developmental profiles of spontaneous activity in cortical and hippocampal cultures. Neural Dev. *10*, 1.

Chévere-Torres, I., Kaphzan, H., Bhattacharya, A., Kang, A., Maki, J.M., Gambello, M.J., Arbiser, J.L., Santini, E., and Klann, E. (2012). Metabotropic glutamate receptor-dependent long-term depression is impaired due to elevated ERK signaling in the ΔRG mouse model of tuberous sclerosis complex. Neurobiol. Dis. *45*, 1101–1110.

Collingridge, G.L., Isaac, J.T., and Wang, Y.T. (2004). Receptor trafficking and synaptic plasticity. Nat. Rev. Neurosci. *5*, 952–962.

Collingridge, G.L., Peineau, S., Howland, J.G., and Wang, Y.T. (2010). Long-term depression in the CNS. Nat. Rev. Neurosci. *11*, 459–473.

Conquet, F., Bashir, Z.I., Davies, C.H., Daniel, H., Ferraguti, F., Bordi, F., Franz-Bacon, K., Reggiani, A., Matarese, V., Condé, F., et al. (1994). Motor deficit and impairment of synaptic plasticity in mice lacking mGluR1. Nature *372*, 237–243.

Daw, M.I., Bortolotto, Z.A., Saulle, E., Zaman, S., Collingridge, G.L., and Isaac, J.T. (2002). Phosphatidylinositol 3 kinase regulates synapse specificity of hippocampal long-term depression. Nat. Neurosci. *5*, 835–836.

Di Prisco, G.V., Huang, W., Buffington, S.A., Hsu, C.C., Bonnen, P.E., Placzek, A.N., Sidrauski, C., Krnjević, K., Kaufman, R.J., Walter, P., and Costa-Mattioli, M. (2014). Translational control of mGluR-dependent long-term depression and object-place learning by eIF2α. Nat. Neurosci. *17*, 1073–1082.

Doherty, A.J., Coutinho, V., Collingridge, G.L., and Henley, J.M. (1999). Rapid internalization and surface expression of a functional, fluorescently tagged G-protein-coupled glutamate receptor. Biochem. J. *341*, 415–422.

Dudek, S.M., and Bear, M.F. (1992). Homosynaptic long-term depression in area CA1 of hippocampus and effects of N-methyl-D-aspartate receptor blockade. Proc. Natl. Acad. Sci. U S A *89*, 4363–4367.

Eales, K.L., Palygin, O., O'Loughlin, T., Rasooli-Nejad, S., Gaestel, M., Müller, J., Collins, D.R., Pankratov, Y., and Corrêa, S.A. (2014). The MK2/3 cascade regulates AMPAR trafficking and cognitive flexibility. Nat. Commun. *5*, 4701.

Ehlers, M.D. (2000). Reinsertion or degradation of AMPA receptors determined by activity-dependent endocytic sorting. Neuron *28*, 511–525.

Fitzjohn, S.M., Kingston, A.E., Lodge, D., and Collingridge, G.L. (1999). DHPG-induced LTD in area CA1 of juvenile rat hippocampus; characterisation and sensitivity to novel mGlu receptor antagonists. Neuropharmacology *38*, 1577–1583.

Fitzjohn, S.M., Palmer, M.J., May, J.E., Neeson, A., Morris, S.A., and Collingridge, G.L. (2001). A characterisation of long-term depression induced by metabotropic glutamate receptor activation in the rat hippocampus in vitro. J. Physiol. *537*, 421–430.

Fiuza, M., Rostosky, C.M., Parkinson, G.T., Bygrave, A.M., Halemani, N., Baptista, M., Milosevic, I., and Hanley, J.G. (2017). PICK1 regulates AMPA receptor endocytosis via direct interactions with AP2 α-appendage and dynamin. J. Cell Biol. *216*, 3323–3338.

Francesconi, A., Kumari, R., and Zukin, R.S. (2009). Regulation of group I metabotropic glutamate receptor trafficking and signaling by the caveolar/lipid raft pathway. J. Neurosci. *29*, 3590–3602.

Gladding, C.M., Fitzjohn, S.M., and Molnár, E. (2009). Metabotropic glutamate receptor-mediated long-term depression: molecular mechanisms. Pharmacol. Rev. *61*, 395–412.

Goh, J.J., and Manahan-Vaughan, D. (2013). Endogenous hippocampal LTD that is enabled by spatial object recognition requires activation of NMDA receptors and the metabotropic glutamate receptor, mGlu5. Hippocampus *23*, 129–138.

Granger, A.J., Shi, Y., Lu, W., Cerpas, M., and Nicoll, R.A. (2013). LTP requires a reserve pool of glutamate receptors independent of subunit type. Nature *493*, 495–500.

Greger, I.H., Khatri, L., and Ziff, E.B. (2002). RNA editing at arg607 controls AMPA receptor exit from the endoplasmic reticulum. Neuron *34*, 759–772.

Greger, I.H., Watson, J.F., and Cull-Candy, S.G. (2017). Structural and Functional Architecture of AMPA-Type Glutamate Receptors and Their Auxiliary Proteins. Neuron *94*, 713–730.

Hardingham, N.R., Read, J.C., Trevelyan, A.J., Nelson, J.C., Jack, J.J., and Bannister, N.J. (2010). Quantal analysis reveals a functional correlation between presynaptic and postsynaptic efficacy in excitatory connections from rat neocortex. J. Neurosci. *30*, 1441–1451.

Hayer, A., Stoeber, M., Bissig, C., and Helenius, A. (2010). Biogenesis of caveolae: stepwise assembly of large caveolin and cavin complexes. Traffic *11*, 361–382.

Henry, F.E., McCartney, A.J., Neely, R., Perez, A.S., Carruthers, C.J., Stuenkel, E.L., Inoki, K., and Sutton, M.A. (2012). Retrograde changes in presynaptic function driven by dendritic mTORC1. J Neurosci *32*, 17128–17142.

Hessler, N.A., Shirke, A.M., and Malinow, R. (1993). The probability of transmitter release at a mammalian central synapse. Nature *366*, 569–572.

Hires, S.A., Zhu, Y., and Tsien, R.Y. (2008). Optical measurement of synaptic glutamate spillover and reuptake by linker optimized glutamate-sensitive fluorescent reporters. Proc. Natl. Acad. Sci. U S A *105*, 4411–4416.

Hong, Y.H., Kim, J.Y., Lee, J.H., Chae, H.G., Jang, S.S., Jeon, J.H., Kim, C.H., Kim, J., and Kim, S.J. (2009). Agonist-induced internalization of mGluR1alpha is mediated by caveolin. J. Neurochem. *111*, 61–71.

Hou, L., and Klann, E. (2004). Activation of the phosphoinositide 3-kinase-Akt-mammalian target of rapamycin signaling pathway is required for metabotropic glutamate receptor-dependent long-term depression. J. Neurosci. *24*, 6352–6361.

Hsieh, H., Boehm, J., Sato, C., Iwatsubo, T., Tomita, T., Sisodia, S., and Malinow, R. (2006). AMPAR removal underlies Abeta-induced synaptic depression and dendritic spine loss. Neuron 52, 831-843.Huber, K.M., Kayser, M.S., and Bear, M.F. (2000). Role for rapid dendritic protein synthesis in hippocampal mGluR-dependent long-term depression. Science *288*, 1254–1257.

Huber, K.M., Kayser, M.S., and Bear, M.F. (2000). Role for rapid dendritic protein synthesis in hippocampal mGluR-dependent long term depression. Science *288*, 1254–1257.

Jakawich, S.K., Nasser, H.B., Strong, M.J., McCartney, A.J., Perez, A.S., Rakesh, N., Carruthers, C.J., and Sutton, M.A. (2010). Local presynaptic activity gates homeostatic changes in presynaptic function driven by dendritic BDNF synthesis. Neuron *68*, 1143–1158.

Jo, J., Son, G.H., Winters, B.L., Kim, M.J., Whitcomb, D.J., Dickinson, B.A., Lee, Y.B., Futai, K., Amici, M., Sheng, M., et al. (2010). Muscarinic receptors induce LTD of NMDAR EPSCs via a mechanism involving hippocalcin, AP2 and PSD-95. Nat. Neurosci. *13*, 1216–1224.

Johnstone, V.P., and Raymond, C.R. (2013). Postsynaptic protein synthesis is required for presynaptic enhancement in persistent forms of long-term potentiation. Front. Synaptic Neurosci. *5*, 1.

Kay, A.R., Alfonso, A., Alford, S., Cline, H.T., Holgado, A.M., Sakmann, B., Snitsarev, V.A., Stricker, T.P., Takahashi, M., and Wu, L.G. (1999). Imaging synaptic activity in intact brain and slices with FM1-43 in C. elegans, lamprey, and rat. Neuron *24*, 809–817.

Kay, L., Humphreys, L., Eickholt, B.J., and Burrone, J. (2011). Neuronal activity drives matching of pre- and postsynaptic function during synapse maturation. Nat. Neurosci. *14*, 688–690.

Kemp, N., and Bashir, Z.I. (1999). Induction of LTD in the adult hippocampus by the synaptic activation of AMPA/kainate and metabotropic glutamate receptors. Neuropharmacology *38*, 495–504.

Kim, J., Goldsberry, M.E., Harmon, T.C., and Freeman, J.H. (2016). Developmental changes in hippocampal CA1 single neuron firing and theta activity during associative learning. PLoS ONE *11*, e0164781.

Kopec, C.D., Li, B., Wei, W., Boehm, J., and Malinow, R. (2006). Glutamate receptor exocytosis and spine enlargement during chemically induced long-term potentiation. J. Neurosci. *26*, 2000–2009.

Lindskog, M., Li, L., Groth, R.D., Poburko, D., Thiagarajan, T.C., Han, X., and Tsien, R.W. (2010). Postsynaptic GluA1 enables acute retrograde enhancement of presynaptic function to coordinate adaptation to synaptic inactivity. Proc Natl Acad Sci U S A *107*, 21806–21811.

Lozovaya, N.A., Kopanitsa, M.V., Boychuk, Y.A., and Krishtal, O.A. (1999). Enhancement of glutamate release uncovers spillover-mediated transmission by N-methyl-D-aspartate receptors in the rat hippocampus. Neuroscience *91*, 1321–1330.

Lu, W., Shi, Y., Jackson, A.C., Bjorgan, K., During, M.J., Sprengel, R., Seeburg, P.H., and Nicoll, R.A. (2009). Subunit composition of synaptic AMPA receptors revealed by a single-cell genetic approach. Neuron *62*, 254–268.

Luján, R., Roberts, J.D., Shigemoto, R., Ohishi, H., and Somogyi, P. (1997). Differential plasma membrane distribution of metabotropic glutamate receptors mGluR1 alpha, mGluR2 and mGluR5, relative to neurotransmitter release sites. J. Chem. Neuroanat. *13*, 219–241.

Lüscher, C., and Huber, K.M. (2010). Group 1 mGluR-dependent synaptic long-term depression: mechanisms and implications for circuitry and disease. Neuron *65*, 445–459.

Malinow, R., and Malenka, R.C. (2002). AMPA receptor trafficking and synaptic plasticity. Annu. Rev. Neurosci. *25*, 103–126.

Mameli, M., Balland, B., Luján, R., and Lüscher, C. (2007). Rapid synthesis and synaptic insertion of GluR2 for mGluR-LTD in the ventral tegmental area. Science *317*, 530–533.

Miesenböck, G., De Angelis, D.A., and Rothman, J.E. (1998). Visualizing secretion and synaptic transmission with pH-sensitive green fluorescent proteins. Nature *394*, 192–195.

Moult, P.R., Gladding, C.M., Sanderson, T.M., Fitzjohn, S.M., Bashir, Z.I., Molnar, E., and Collingridge, G.L. (2006). Tyrosine phosphatases regulate AMPA receptor trafficking during metabotropic glutamate receptor-mediated long-term depression. J. Neurosci. *26*, 2544–2554.

Murthy, V.N., Sejnowski, T.J., and Stevens, C.F. (1997). Heterogeneous release properties of visualized individual hippocampal synapses. Neuron *18*, 599–612.

Nadif Kasri, N., Nakano-Kobayashi, A., and Van Aelst, L. (2011). Rapid synthesis of the X-linked mental retardation protein OPHN1 mediates mGluR-dependent LTD through interaction with the endocytic machinery. Neuron *72*, 300–315.

O'Brien, J.A., and Lummis, S.C. (2006). Diolistic labeling of neuronal cultures and intact tissue using a hand-held gene gun. Nat. Protoc. *1*, 1517–1521.

Okuno, H., Akashi, K., Ishii, Y., Yagishita-Kyo, N., Suzuki, K., Nonaka, M., Kawashima, T., Fujii, H., Takemoto-Kimura, S., Abe, M., et al. (2012). Inverse synaptic tagging of inactive synapses via dynamic interaction of Arc/Arg3.1 with CaMKIIβ. Cell *149*, 886–898.

Oliet, S.H., Malenka, R.C., and Nicoll, R.A. (1997). Two distinct forms of long-term depression coexist in CA1 hippocampal pyramidal cells. Neuron *18*, 969–982.

Palmer, M.J., Irving, A.J., Seabrook, G.R., Jane, D.E., and Collingridge, G.L. (1997). The group I mGlu receptor agonist DHPG induces a novel form of LTD in the CA1 region of the hippocampus. Neuropharmacology *36*, 1517–1532.

Palmer, M.J., Isaac, J.T., and Collingridge, G.L. (2004). Multiple, developmentally regulated expression mechanisms of long-term potentiation at CA1 synapses. J. Neurosci. *24*, 4903–4911.

Pula, G., Mundell, S.J., Roberts, P.J., and Kelly, E. (2004). Agonist-independent internalization of metabotropic glutamate receptor 1a is arrestin- and clathrin-dependent and is suppressed by receptor inverse agonists. J. Neurochem. *89*, 1009–1020.

Pyle, J.L., Kavalali, E.T., Choi, S., and Tsien, R.W. (1999). Visualization of synaptic activity in hippocampal slices with FM1-43 enabled by fluorescence quenching. Neuron *24*, 803–808.

Rathje, M., Fang, H., Bachman, J.L., Anggono, V., Gether, U., Huganir, R.L., and Madsen, K.L. (2013). AMPA receptor pHluorin-GluA2 reports NMDA receptor-induced intracellular acidification in hippocampal neurons. Proc. Natl. Acad. Sci. U S A *110*, 14426–14431.

RichmondRichmond, S.A., Irving, A.J., Molnar, E., McIlhinney, R.A., Michelangeli, F., Henley, J.M., and Collingridge, G.L. (1996). Localization of the glutamate receptor subunit GluR1 on the surface of living and within cultured hippocampal neurons. Neuroscience *75*, 69–82.

Rocca, D.L., Amici, M., Antoniou, A., Blanco Suarez, E., Halemani, N., Murk, K., McGarvey, J., Jaafari, N., Mellor, J.R., Collingridge, G.L., and Hanley, J.G. (2013). The small GTPase Arf1 modulates Arp2/3-mediated actin polymerization via PICK1 to regulate synaptic plasticity. Neuron *79*, 293–307.

Roh, S.E., Hong, Y.H., Jang, D.C., Kim, J., and Kim, S.J. (2014). Lipid rafts serve as signaling platforms for mGlu1 receptor-mediated calcium signaling in association with caveolin. Mol. Brain *7*, 9.

Rosenmund, C., Clements, J.D., and Westbrook, G.L. (1993). Nonuniform probability of glutamate release at a hippocampal synapse. Science *262*, 754–757.

Roth, R.H., Zhang, Y., and Huganir, R.L. (2017). Dynamic imaging of AMPA receptor trafficking in vitro and in vivo. Curr. Opin. Neurobiol. *45*, 51–58.

Ryan, T.A., Reuter, H., Wendland, B., Schweizer, F.E., Tsien, R.W., and Smith, S.J. (1993). The kinetics of synaptic vesicle recycling measured at single presynaptic boutons. Neuron *11*, 713–724.

Sanderson, T.M., Collingridge, G.L., and Fitzjohn, S.M. (2011). Differential trafficking of AMPA receptors following activation of NMDA receptors and mGluRs. Mol. Brain *4*, 30.

Schindelin, J., Arganda-Carreras, I., Frise, E., Kaynig, V., Longair, M., Pietzsch, T., Preibisch, S., Rueden, C., Saalfeld, S., Schmid, B., et al. (2012). Fiji: an open-source platform for biological-image analysis. Nat. Methods *9*, 676–682.

Schnabel, R., Kilpatrick, I.C., and Collingridge, G.L. (1999). An investigation into signal transduction mechanisms involved in DHPG-induced LTD in the CA1 region of the hippocampus. Neuropharmacology *38*, 1585–1596.

Scholz, R., Berberich, S., Rathgeber, L., Kolleker, A., Köhr, G., and Kornau, H.C. (2010). AMPA receptor signaling through BRAG2 and Arf6 critical for long-term synaptic depression. Neuron *66*, 768–780.

Snyder, E.M., Philpot, B.D., Huber, K.M., Dong, X., Fallon, J.R., and Bear, M.F. (2001). Internalization of ionotropic glutamate receptors in response to mGluR activation. Nat. Neurosci. *4*, 1079–1085.

Takayasu, Y., Takeuchi, K., Kumari, R., Bennett, M.V., Zukin, R.S., and Francesconi, A. (2010). Caveolin-1 knockout mice exhibit impaired induction of mGluR-dependent long-term depression at CA3-CA1 synapses. Proc. Natl. Acad. Sci. U S A *107*, 21778–21783.

Thiagarajan, T.C., Lindskog, M., and Tsien, R.W. (2005). Adaptation to synaptic inactivity in hippocampal neurons. Neuron *47*, 725–737.

Tokuoka, H., and Goda, Y. (2008). Activity-dependent coordination of presynaptic release probability and postsynaptic GluR2 abundance at single synapses. Proc. Natl. Acad. Sci. U S A *105*, 14656–14661.

Volk, L.J., Daly, C.A., and Huber, K.M. (2006). Differential roles for group 1 mGluR subtypes in induction and expression of chemically induced hippocampal long-term depression. J. Neurophysiol. *95*, 2427–2438.

Watabe, A.M., Carlisle, H.J., and O'Dell, T.J. (2002). Postsynaptic induction and presynaptic expression of group 1 mGluR-dependent LTD in the hippocampal CA1 region. J. Neurophysiol. *87*, 1395–1403.

Waung, M.W., Pfeiffer, B.E., Nosyreva, E.D., Ronesi, J.A., and Huber, K.M. (2008). Rapid translation of Arc/Arg3.1 selectively mediates mGluR-dependent LTD through persistent increases in AMPAR endocytosis rate. Neuron *59*, 84–97.

Wenthold, R.J., Petralia, R.S., Blahos J, I.I., and Niedzielski, A.S. (1996). Evidence for multiple AMPA receptor complexes in hippocampal CA1/CA2 neurons. J. Neurosci. *16*, 1982–1989.

Wilkinson, K.A., Ashby, M.C., and Henley, J.M. (2014). Validity of pHluorin-tagged GluA2 as a reporter for AMPA receptor surface expression and endocytosis. Proc. Natl. Acad. Sci. U S A *111*, E304.

Williams, J.H., Errington, M.L., Lynch, M.A., and Bliss, T.V. (1989). Arachidonic acid induces a long-term activity-dependent enhancement of synaptic transmission in the hippocampus. Nature *341*, 739–742.

Xiao, M.Y., Zhou, Q., and Nicoll, R.A. (2001). Metabotropic glutamate receptor activation causes a rapid redistribution of AMPA receptors. Neuropharmacology *41*, 664–671.

Zhou, Z., Hu, J., Passafaro, M., Xie, W., and Jia, Z. (2011). GluA2 (GluR2) regulates metabotropic glutamate receptor-dependent long-term depression through N-cadherin-dependent and cofilin-mediated actin reorganization. J. Neurosci. *31*, 819–833.

Zhuo, M., Small, S.A., Kandel, E.R., and Hawkins, R.D. (1993). Nitric oxide and carbon monoxide produce activity-dependent long-term synaptic enhancement in hippocampus. Science *260*, 1946–1950.

STAR★METHODS

KEY RESOURCES TABLE

REAGENT or RESOURCE	SOURCE	IDENTIFIER
Chemicals, Peptides, and Recombinant Proteins		
RS-DHPG	Tocris/HelloBio	*Cat# 0342/1 or HB0026*
L-689,560	Tocris	Cat# 0742/10
LY-367385	Tocris/HelloBio	Cat# 1237/10 or HB0398
YM 298198 hydrochloride	Tocris/HelloBio	Cat# 2448/10 or HB0664
MPEP hydrochloride	Tocris	Cat# 1212/10
NMDA	Tocris	Cat# 0114/50
4-Aminopyridine	Tocris	Cat# 0940/100
TBOA	Tocris	Cat# 1223/10 or HB0258
Picrotoxin	Tocris/HelloBio	Cat# 1128/1G or HB0506
FM4-64	Life Technologies	Cat# T13320
ADVASEP-7	Biotium	Cat# 70029
2-chloroadenosine	Santa Cruz Biotechnology	Cat# sc-203768
QX 314 chloride	Tocris/HelloBio	Cat# 2313/50 or HB1030
Minimal essential media with Hank's salts	Life Technologies	*Cat# 11575032*
Horse serum	Life Technologies	Cat# 26050088
L-Ascorbic acid	Sigma	Cat# A5960
Insulin	Sigma	Cat# I6634
Spermidine	Sigma	Cat# S0266
Polyvinylpyrollidone	Sigma	Cat# PVP360
Critical Commercial Assays		
QIAGEN Plasmid Maxi Kit	QIAGEN	Cat# 12163
Experimental Models: Organisms/Strains		
CD® (Sprague Dawley) IGS Rat	Charles River	001
Recombinant DNA		
pCI-SEP-GluA2(Q)	Kopec et al., 2006	Addgene Cat# 24002
SEP-mGluR1α	Roh et al., 2014	N/A
SEP-mGluR1(F609,614A)	Roh et al., 2014	N/A
EGFP-Cav1	Hayer et al., 2010	Addgene Cat# 27704
Software and Algorithms		
WinLTP	Anderson and Collingridge, 2007; Anderson et al., 2012	https://www.winltp.com/
Fiji	Schindelin et al., 2012	http://fiji.sc/
Time series analyzer (plugin for ImageJ)	Schindelin et al., 2012	http://rsb.info.nih.gov/ij/plugins/time-series.html
SigmaPlot 12.5	Systat Software Inc.	https://systatsoftware.com/downloads/download-sigmaplot/
MiniAnalysis	Synaptosoft Inc.	http://www.synaptosoft.com/MiniAnalysis/index.html

CONTACT FOR REAGENT AND RESOURCE SHARING

Further information and requests for resources and reagents should be directed to and will be fulfilled by the Lead Contact, Graham L. Collingridge (glcollingridge@gmail.com).

EXPERIMENTAL MODEL AND SUBJECT DETAILS

Preparation of organotypic culture

Organotypic hippocampal slices were prepared as described previously (Rocca et al., 2013). Briefly, male P7 SD rats were sacrificed by cervical dissociation in accordance with the UK animals (Scientific procedures) act 1986 and the South Korean Animal Protection act, 1991. Hippocampi were removed and 350 μm thick slices were prepared using a Leica VT 1200 S vibratome (Leica microsystems, Germany). Slicing was performed in cutting solution containing (in mM) Sucrose (238); KCl (2.5); D-glucose (11); $NaHCO_3$ (26); NaH_2PO_4 (1); $CaCl_2$ (1) and $MgSO_4$ (5). Slices were then washed in filtered culture media containing 78.8% minimal essential media (MEM) with Hank's salts; 20% horse serum; HEPES (30); D-glucose (16); $NaHCO_3$ (5); $CaCl_2$ (1); $MgSO_4$ (2); L-ascorbic acid (0.68) and insulin (1 μg/ml). Slices were then placed on sterile 30 mm Millicell cell culture inserts (0.4 μm pore size, Millipore, Ireland) resting on culture media and maintained at 35°C in 5% CO_2. All equipment was sterilized before use. Media was changed every 2 days. Slices were used at 2-3 weeks *in vitro*.

METHOD DETAILS

Biolistic transfection

Plasmid DNA was amplified using QIAGEN Plasmid Maxi Kits (QIAGEN, Manchester, UK). Gene gun bullets were prepared as described previously (O'Brien and Lummis, 2006). In brief, spermidine (0.05 M), plasmid DNA and calcium chloride (1 M) were added to 1 μm diameter gold micro carriers (in that order) and incubated at room temperature for 10 min with intermittent agitation. 1-10 μg of DNA was added per mg of gold. Gold bullets were then washed with pure ethanol 3 times and suspended in polyvinylpyrrolidone (PVP) solution in ethanol (75 μg/ml). This solution was transferred to Tefzel tubing, the gold bullets were allowed to sediment at the bottom of the tube and the remaining solution was removed. Rotation of the tube caused its interstices to be coated with gold bullets and flow of nitrogen through the tube dried the bullets in place. The gold bullet coated tubing was segmented into 1 cm pieces, such that 0.2-0.5 mg of DNA coated gold particles were in each segment, and the gold bullets were fired at organotypic slices using a Helios gene gun (Biorad, CA, USA) with 140 psi helium. Organotypic slices were transfected after 1 week in culture, and were used in experiments at 2-3 weeks in culture.

Patch clamp electrophysiology

Patch clamp electrophysiological recordings were performed on organotypic hippocampal slices. In brief, slices were transferred to a recording chamber and continuously perfused with artificial cerebral spinal fluid (ACSF) containing (in mM): NaCl (119); KCl (2.5); D-glucose (11); $NaHCO_3$ (26); NaH_2PO_4 (1); $CaCl_2$ (4); $MgCl_2$ (4); picrotoxin (0.05) and 2-chloroadenosine (0.01) at 2 ml/min, heated using an inline heater to 33°C. 2-chloroadenosine was included to reduce excitability. Patch electrodes (~3-5 MΩ) were used that contained whole-cell solution comprised of (in mM): cesium-methane sulphonate (130); HEPES (10); EGTA (0.5); NaCl (8); Mg-ATP (4); Na_2-GTP (0.3); QX314 (6); ~290 mOsm; pH adjusted to 7.2 using CsOH. The initial offset potential was corrected before recording and cells were held at −70 mV. Recordings were sampled at 20 kHz using WinLTP (Anderson and Collingridge, 2007; Anderson et al., 2012), filtered at 2 kHz and series resistance was measured at 30 s intervals throughout recordings. Recordings in which the series resistance varied by < 20% were accepted for analysis. Evoked EPSCs were analyzed offline using WinLTP. For AMPAR mediated synaptic transmission peak responses at −70 mV were measured. For NMDAR mediated synaptic transmission responses 60 ms following stimulation at 40 mV were measured.

EGFP and SEP imaging

CA1 pyramidal cells were transfected as described above and maintained in the same conditions as outlined for patch clamp experiments, except where the effect of LFS on SEP-GluA2 fluorescence was tested, where $CaCl_2$ (2) and $MgCl_2$ (1) were used, in order to facilitate the induction of NMDAR-dependent LTD. Control experiments were also performed in these conditions and found to be identical to those performed in $CaCl_2$ (4) and $MgCl_2$ (4) (included in Figure 3D-F). Electrical stimulation at baseline frequency was applied during imaging experiments where DHPG was applied and during interleaved controls, to ensure consistency with electrophysiological experiments. Similar to other studies that image SEP-GluA2 in organotypic slices (Kopec et al., 2006; Hsieh et al., 2006), we used the unedited version (SEP-GluA2-607Q) as this produced fluorescence with a sufficient signal to noise ratio for imaging studies (10 ± 3; n = 7), whereas the edited version (SEP-GluA2-607R) did not (1.6 ± 0.1; n = 6). SEP-GluA2-607Q was a gift from Roberto Malinow. Images of living neurons were acquired using a 63 × water-immersion objective lens (numerical aperture, 1.2) of a Zeiss LSM 7 MP (Zeiss, Oberkochen, Germany) in combination with a Chameleon Coherent Vision II multiphoton laser (Coherent, CA, USA). For some experiments, a Biorad Radiance 2100 multi-photon installation (Zeiss, Oberkochen, Germany) in combination with a Mai Tai multiphoton laser (Spectra Physics, Mountain View, CA, USA) or an Olympus FV1200MPE (Olympus, Southend-on-sea, UK) in combination with a Mai Tai DeepSee multiphoton laser (Spectra Physics, Mountain View, CA, USA) was used. An excitation wavelength of 900 nm was used in all setups. The minimum light intensity was used that resulted in adequate signal to noise ratio to prevent photo damage to neurons. The range of laser intensities used were between 20 mW and 70 mW, measured at the back aperture of the objective lens using a Spectraphysics Model 407A power meter (Spectra Physics, Mountain View, CA, USA). Also, the total number of images was kept to the minimum so that bleaching was negligible. Image stacks consisting of 1 μm axial z-steps were constructed.

For analysis of SEP fluorescence, average z projected images were constructed from the image stacks and regions of interest (ROIs) were placed over fluorescent puncta. Small movements of dendrites or spines were compensated for by replacing the regions of interest manually at each time point. The level of AMPAR internalization was estimated for each neuron by averaging the intensity change within ROIs. The changes at individual synapses were quantified using cumulative likelihood distributions.

FM4-64 imaging

Pre-synaptic boutons in organotypic slices were loaded with FM4-64 using a method described previously (Johnstone and Raymond, 2013; Kay et al., 1999; Murthy et al., 1997). In brief, FM4-64 (5 μM) was washed into the slice and loaded into presynaptic boutons by simulating the Schaffer collateral pathway 100 times at 0.16 Hz. This labeling occurs because vesicular neurotransmitter release induced by stimulation of Schaffer collaterals (STIM; Figure 2A) is followed by the formation of replacement vesicles, manufactured from the external cell membrane. FM labels external membranes and so vesicles formed in the presence of FM are therefore also labeled. Washout of FM from external cell membranes, facilitated by ADVASEP-7 (0.5 mM) for 5 min followed by a further 30 min wash in ACSF (Figure 2A) restricts FM labeling to only those internalized membranes that form new vesicles.

Prior to dye loading the stimulation strength was set by patching onto a neuron neighboring the SEP expressing neuron under study, such that an EPSC of size 100-400 pA was obtained with no sign of epileptiform activity. This results in a relatively low density of labeling by FM4-64 which is representative of the relatively small number of synapses that contribute to synaptic responses evoked in this way. FM4-64-labeled synapses were imaged using the Zeiss LSM 7 MP or the Olympus FV1200MPE. The excitation parameters were optimized such that the range of FM4-64 fluorescence corresponded to the range over which the GaAsP detector was sensitive. Thus, in our conditions the fluorescence from the brightest FM4-64 puncta, corresponding to synapses with high P(r), did not saturate the detector, while very low intensity FM4-64 puncta, corresponding to low P(r) synapses, could still be detected. To obtain this working range in FM4-64 fluorescence it was necessary to use a lower energy to excite the fluorophores compared to when SEP was used alone. This resulted in less intense SEP fluorescence when used in combination with FM4-64 (Figure 2B, 3A-C, 3J-K, 4A and 6A-C) compared to when SEP was used alone (Figure 1E and I, 5B, D and J and Figure S4). These excitation parameters (24 mW of 900 nm light from the Chameleon Coherent Vision II multiphoton laser or the Mai Tai DeepSee multiphoton laser with constant gain and offset) were kept constant. Variations in the maximum output of the laser were corrected for by changing the percentage of laser power utilized. To verify that FM4-64 puncta represent pre-synaptic boutons labeled as a result of the electrical stimulation provided, as opposed to non-specific uptake of dye, further stimulation of the Schaffer collaterals were delivered to de-stain such bona fide pre-synaptic boutons. This protocol was confirmed to have no effect on synaptic transmission by patch clamp experiments (not shown). Only FM4-64 puncta that had diminished fluorescence were accepted for analysis.

P(r) was calculated according to the method described in Murthy et al., 1997. First, the fluorescence intensity that corresponds to 1 stained vesicle is measured by presenting the FM4-64 puncta fluorescence intensity in a frequency histogram with bin sizes that are expected to be below the fluorescence intensity of a single synaptic vesicle. This treatment results in multiple peaks, which are separated by a value that corresponds to the fluorescence of a single synaptic vesicle (c). Therefore, the maximum fluorescence that can be achieved after *i* stimulations is *ci.* The P(r) of any given pre-synaptic puncta is equal to the fluorescence intensity of that puncta after *i* stimulations (F*i*) divided by c*i*. (P(r) = F*i*/c*i*).

Where SEP-GluA2(Q), SEP-mGluR1, SEP-mGluR1(F609,614A) or Cav-EGFP were imaged in combination with FM4-64, green fluorescence changes of SEP puncta adjacent to red FM4-64 puncta were analyzed as above. In addition, to compare the relative basal fluorescence intensity with respect to P(r), the green SEP fluorescence was normalized to the mean (F/F_{mean}). Histograms were constructed to graphically show the distribution of the SEP fluorescence change according to P(r); in some cases the average SEP changes were further compared through bar plots of binned P(r) ranges. In these cases, multiple ROIs from within single neurons were sampled, and the data were first averaged on a per-neuron basis, such that the *n* repetitions shown represents the number of neurons.

QUANTIFICATION AND STATISTICAL ANALYSIS

Statistical details of experiments including the definition of n, the center, dispersion and precision measurements, can be found in the results section. In summary, for comparisons between conditions, data were normalized and significance was determined using one way analysis of variance (ANOVA) followed post hoc by the Bonferroni correction. Comparisons between baseline values and values 30 min post DHPG were performed on raw data using Student's t tests. Correlations were determined by measuring Spearman's rank correlation coefficients. The level of significance was set at $p < 0.05$.

DATA AND SOFTWARE AVAILABILITY

Electrophysiological data were analyzed using WinLTP (Anderson and Collingridge, 2007; Anderson et al., 2012; https://www.winltp.com/). Imaging data were analyzed using the time series analyzer (Schindelin et al., 2012; http://rsb.info.nih.gov/ij/plugins/time-series.html) plugin of Fiji (http://fiji.sc/). Statistical tests were performed using SigmaPlot 12.5 (Systat Software Inc., San Jose, CA, USA; https://systatsoftware.com/downloads/download-sigmaplot/) or where Kolmogorov-Smirnov tests were applied using MiniAnalysis (Synaptosoft Inc., Decatur, GA, USA; http://www.synaptosoft.com/MiniAnalysis/index.html).